Peptide Synthesis (Solid-Phase Method)

The oligopeptide without free amino- or carboxyl end was synthesized based on the Fmoc (9-fluorenyl-methyloxycarbonyl group) strategy. A solid support of an Fmoc-protected super acid-labile polyethyleneglycol resin (Fmoc-NH-SAL PEG, Watanabe Chem., Japan) was used for the solid support synthesis. After removal of the Fmoc group by piperidine, an Fmoc L-amino acid (Watanabe Chem.) activated by 3 molar amounts of HATU [*O*-(7-azabenzotriazol-1-yl) *N,N,N',N'*-tetramethyluronium hexafluorophosphate], 3 molar amounts of HOAt (1-Hydroxy-7-azabenzotriazole), and 6 molar amounts of DIPEA (*N,N*-diisopropylethylamine) was coupled to the resin. The amino acids were sequentially coupled to the resin, and the unreacted amino terminus in each coupling step was capped with acetic anhydride. The fully elongated oligopeptide was further treated with acetic anhydride after removing the Fmoc group. The synthesized oligopeptide was cleaved from the resin and deblocked by trifluoroacetic acid mixed with *m*-cresol, 1,2-ethanediol, thioanisole, and trimethylsilyl bromide. The deblocked peptide was purified by reversed-phase HPLC using an acetonitrile gradient (Tosoh, Japan), and the molecular weight of the peptide was confirmed by MALDI-TOF mass spectrometry (Applied Biosystems, Foster City, CA). The oligopeptide concentration was determined by the UV absorbance of the tyrosine residue attached at the N-terminal end of the sequence.

NPCs Obtained from E12 Rat Embryos and Cell Culture

The preparation and culturing of NPCs were slightly modified from the previously described methods [37]. Embryonic E12 fetuses were obtained from anesthetized pregnant Sprague-Dawley rats (SLC, Hamamatsu, Japan). Tissues from the forebrain and hindbrain were dissected, digested with 0.05% trypsin and 0.02% ethylenediamine tetraacetic acid at 37°C for 10 min, dissociated by gentle trituration in DMEM/F12 (Invitrogen, Carlsbad, CA), and filtered through a sterile 60-mesh membrane. The cells were then centrifuged and resuspended in serum-free DMEM/F12 supplemented with glucose (0.6%), glutamine (2 mM), $NaHCO_3$ (3 mM), insulin (25 μg/ml), transferrin (100 μg/ml), progesterone (20 mM), putrescine (60 μM), selenium chloride (30 mM), and HEPES buffer (pH 7.4). Epidermal growth factor (Upstate Biotechnology, Lake Placid, NY) and basic fibroblast growth factor (PeproTech, London, UK) were added either alone or in combination at concentrations of 10^{-11} and 10^{-9} M, respectively.

Intracellular Delivery of Synthetic Peptide by BioPorter

For intracellular delivery of the peptide, BioPorter lipid reagent encapsulating molecules were used. BioPorter lipid reagent containing a trifluoroacetylated lipopolyamine mixed with dioleoyl phosphatidylethanolamine was obtained from Gene Therapy Systems, Inc. (San Diego, CA). According to the manufacturer's instructions, 100 μl of the hydrated mixture containing the VHL 156-171 peptide, trifluoroacetylated lipopolyamine, and diloeoyl phosphatidylethanolamine (BioPorter) was diluted in 100 μl of serum-free medium and added to the cells. The BioPorter-peptide complexes became attached to the negatively charged cell surface and fused with it, allowing the captured protein to be delivered into the cells. As controls, the above-stated amount of BioPorter without the peptide and two kinds of peptide mutants, L158V and C162F were used.

The medium containing the complexes was replaced with 1% serum-containing DMEM/F12 medium after a 4-hour incubation at 37°C. Intracellular delivery of the peptide were confirmed by using fluorescently labeled peptide. The peptides were fluorescently labeled with Alexa Fluor-594 by using an Alexa Fluor-594 Labeling Kit (Molecular Probes, Eugene, OR). Cells were cultured on Lab-Tech IV chamber slides (NUNC, Rochester, NY) for 24 h. Then Alexa Fluor-594-labeled peptide mixed with BioPorter reagent was then added to the cells as described above. At 24 h, the cells were washed 3 times in PBS; and the live unfixed cells were observed by using a confocal laser microscope FV300 (Olympus, Tokyo, Japan).

Morphological change in NPCs (Neurite Outgrowth)

To examine the morphological change for neuronal differentiation after the intracellular delivery of the peptides or non-peptide, a NSC showing neurite outgrowth >5μm was evaluated as a neuronal differentiated NSC. We determined the rate of NPCs showing neurite outgrowth by observing the 200 cells by phase-contrast microscopy at 4, 8, 12, 24, 48, 72, and 96 hours after the addition of the peptide–lipid complexes at a 0.3, 3, and 30 μM concentrations.

Immunocytochemical Studies

At 0, 24, 48, 72, and 92 hours after the addition of the complexes at 3μM concentration, the cells on coverslips were fixed for 30 seconds in cold acetone (4°C), cooled quickly in a deep freezer (-80°C), and maintained at -80°C prior to immunostaining. The cells were blocked with 5% normal donkey serum (NDS) in phosphate-buffered saline (PBS) and then exposed to either mouse mAb specific for microtubules associated protein (MAP)-2 (1:200; Sigma, St. Louis, MO) or rabbit polyclonal antibody (pAb) specific for glial fibrillary acidic protein (GFAP) (1:200; Sigma) as the primary antibody. Controls consisted of staining with 5% NDS in PBS from which the primary antibody had been omitted. Secondary antibody staining consisted of exposure for 30 min at 37°C to swine anti-mouse or anti-rabbit immunoglobulin conjugated to rhodamine (1:100). Coverslips were mounted onto slides and viewed. The rate of NPCs positive for each of these marker proteins was then determined.

Electrophysiology

To record fast sodium and delayed rectifier potassium currents, we prepared the extracellular and intracellular solutions as described previously [38]. Two days after the addition of VHL156-171 peptide at 3μM concentration or the addition of non-peptide, a holding potential of -80 mV and voltage step of 20 mV over the range of -100 to 100 mV with 50 msec durations were applied to the recorded cells through patch electrodes. For recordings and data analysis we used CEZ-2300 (Nihon Kohden, Tokyo, Japan) and pCLAMP 6.0 software (Axon Instruments, Burlingame, CA). Linear components of leak and capacitive currents were reduced by ana-

logue circuitry and then canceled by the P/N method. Signals were sampled every 20 μsec, and currents were filtered at 5 kHz. Data were additionally processed with Origin 5.0 (Microcal, Northhampton, MA).

RESULTS

The VHL156-171(YTLKERCLQVVRSLVK) and the peptide mutants, L158V (YTVKERCLQVVRSLVK) and C162F (YTLKERFLQVVRSLVK), were synthesized and purified >95 % by the reversed-phase HPLC. The intracellular delivery of those peptides to the NPCs was performed by using a mixture of the peptide, trifluoroacetylated lipopolyamine, and diloeoyl phosphatidylethanolamine (BioPorter reagent) and was confirmed at 24 hours after the addition of fluorescently labeled BioPorter–peptide complexes. The induction of neuronal differentiation of the NPCs was examined by assessing neurite outgrowth, the expression of neuronal cell-specific markers, and electrophysiological findings. Four to 96 hours after the intracellular delivery, neurite outgrowth from NPCs was observed when the VHL156-171 peptide was used at a 0.3, 3, and 30 μM concentrations. On the other hand, the rate of peptide mutants(L158V, C162F) or non-peptide-delivered NPCs showing neurite outgrowth was significantly much lower at 8, 12, 24, 48, 72, and 96 hours after the addition of the peptides or non-peptide. The morphological changes at 24 hours after the intracellular delivery of the VHL156-171 peptide and control peptides (peptide mutants L158V, C168F) or non-peptide were shown in Fig. (**1**). The VHL156-171 peptide-delivered NPCs mostly showed neurite outgrowth, while peptide mutants or non-peptide-delivered NPCs did not. The time courses of the rate of the cells showing neurite outgrowth are shown in Fig. (**2**). The maximal rate of the cells showing neurite outgrowth was found at 72 hours after the intracellular delivery of VHL156-171 pepitde.

In the immunocytochemical study, the VHL 156-171 pepide- delivered NPCs showed increased expression of neural marker Map2, but decreased expression of the glial marker GFAP (Fig. **3**). On the other hand, the non-peptide or the peptide mutants -delivered cells showed increased expression of GFAP rather than Map2 and actually rarely showed expression of Map2. The time courses of the expression of these marker proteins (Map2, GFAP) are shown in Fig. (**4**). Compared with the expression in control NPCs (the non-peptide- or the peptide mutants-delivered NSCs), Map2 expression increased in VHL156-171 peptide-delivered cells, whereas GFAP expression decreased in them.

Voltage-gated inward and outward currents were recorded in the whole-cell patch-clamp configuration. In whole-cell recordings of VHL156-171 peptide-delivered NPCs showing neurite outgrowth, the depolarizing voltage steps elicited both large outward potassium currents and fast inward Na^+ currents, which are hallmark features of differentiated neurons. On the other hand, in the whole-cell recording of non-peptide-delivered cells without neurite outgrowth, both outward potassium and inward Na+ currents were not elicited (Fig. **5**).

DISCUSSION

Intracellular delivery of protein is superior to the gene transfer with respect to safety, rapidness [7], lack of bio-

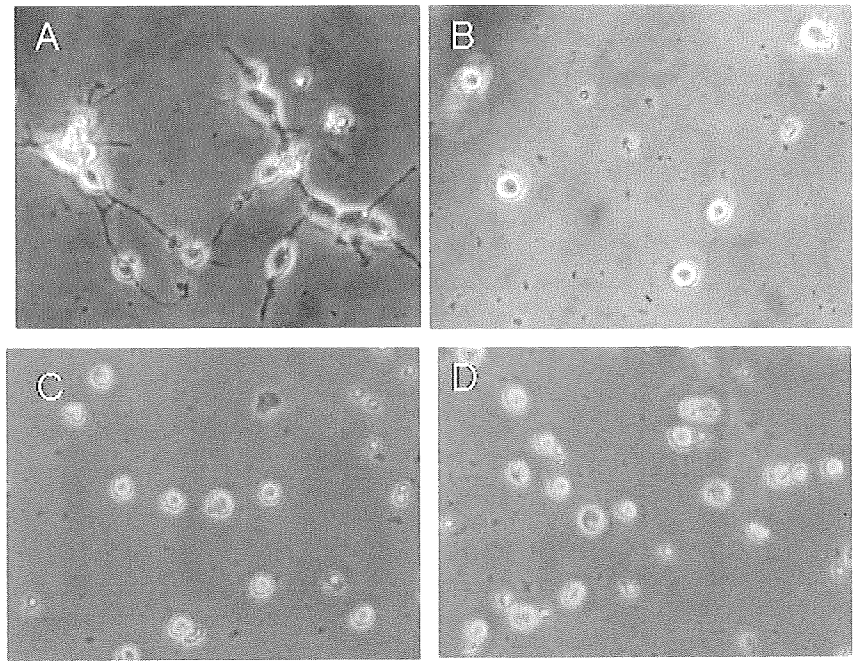

Figure 1. Morphological features of NPCs 24 after the intracellular delivery of the peptides at 3μM concentration or non-peptide. A, NPCs treated with VHL156-171 peptide. Most cells show neurite outgrowth. B, Control NPCs treated with non-peptide (BioPorter). No cells show neurite growth. C, NPCs treated with L158V peptide. No cells show neurite growth. D, NPCs treated with C162F peptide. No cells show neurite growth.

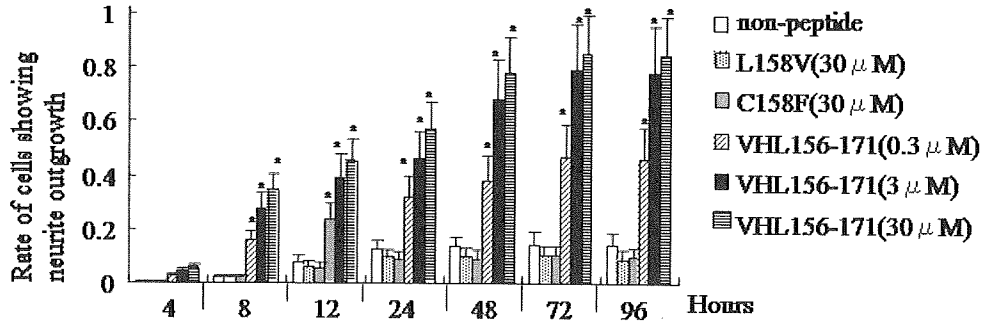

Figure 2. Rate of NPCs having neurite outgrowth after the intracellular delivery of the peptides and non-peptide. The rate of NPCs having neurite outgrowth showed significantly greater in VHL156-171 peptide-delivered NPCs than L158V- or C162F- peptide-delivered NPCs and non-peptide-delivered NPCs. Values are means±SEM. *p<0.01, compared with controls.

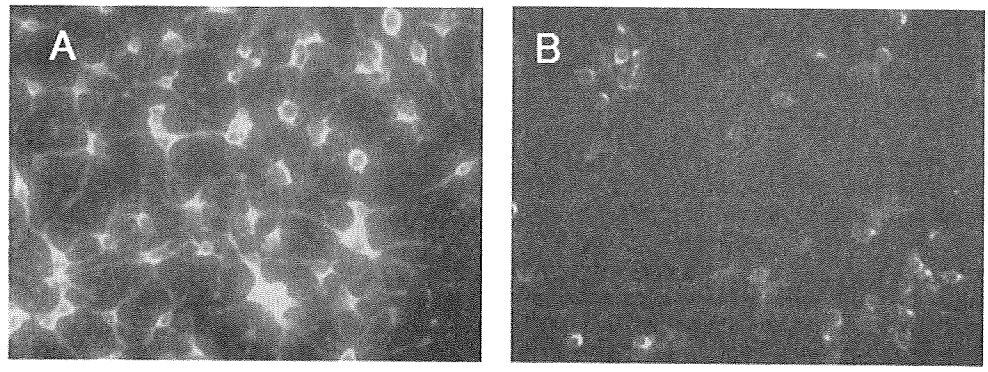

Figure 3. Immunocytochemistry of NPCs at 72 hours after treatment with VHL156-171-peptide. A, Expression of Map2, a neuronal marker. The majority of the cells are positive for Map2. B, Expression of GFAP, an astroglial marker. The minority of the cells show positive for GFAP.

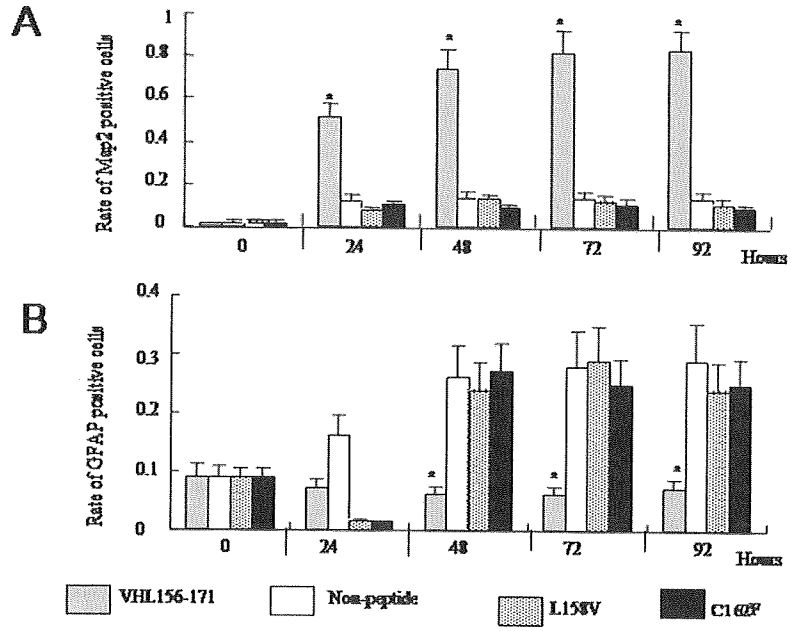

Figure 4. Rate of NPCs expressing cell-specific markers after delivery of the peptides to the cells. A, Rate of NPCs expressing the neuronal marker Map2. VHL 156-171-delivered cells showed a higher positive rate for Map2 than L158V-, C162F-, or non-peptide-delivered NPCs. B, Rate of NPCs expressing GFAP, an astroglial marker. VHL 156-171-delivered cells showed a significantly lower positive rate for GFAP than L158V or C162F-delivered cells and non-delivered cells. Values are means ± SEM. *p<0.01, compared with controls.

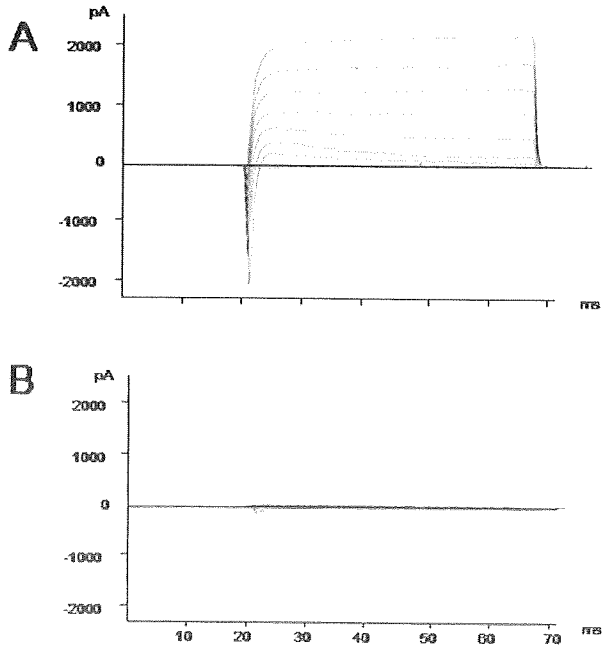

Figure 5. Electrophysiological properties of VHL-peptide delivered NP cells. Voltage-gated inward and outward currents were recorded in the whole-cell patch-clamp configuration. A, VHL156-171-delivered NPCs. Shown in the graph are large outward K^+ currents and fast inward Na^+ currents elicited by depolarizing voltage steps, which is characteristic feature of a mature neuron. B, non-delivered NCS. Both outward K^+ currents and fast inward Na^+ currents are not shown.

ethical problems, little cell toxicity, and no carcinogenesis [39, 40]. In addition, our employed approach for protein transfer using BioPorter has advantages over the other protein delivery approach using protein-transduction domain (PTD) which is derived from HIV-TAT [41] or antenapedia [42], because it does not require modification of the intracellular delivered protein and the efficacy of delivery does not depend on the protein delivered. An oligopeptide, which consists of less than 20 amino-acids, can be chemically composed and used for the intracellular delivery with more facility. However, the functional oligopeptides that show effects similar to those of the full-length proteins expressed by gene transfer are few [6, 7].

The intracellular delivery of a peptide by BioPorter reaches its maximum by 4 hours, and the peptide disappears from the cells after 48 hours [39]. Since the peptide does not remain in the cells, direct intracellular delivery of the peptide has an effect of short duration only on them. Cellular differentiation usually takes place over a long duration of time. In NPCs, however, a short duration of the presence of the peptide was sufficient to trigger the neuronal differentiation of these cells. In addition, the differentiation effected by the intracellular delivery of VHL156-171 occurred at a low concentration of the peptide. When an intracellularly delivered protein has an anti-proliferative effect on cancer cells, this effect is manifested at higher rather than lower concentrations of the protein [40]. Those sufficient effects of short duration and low concentration in the case of NPCs may indicate that the delivered peptide merely plays a critical role as a switch in deciding the direction of differentiation. The peptide composed of our employed amino-acid sequence, VHL 156-171, binds to elongin C, to which elongin A also binds. In the crystal structure, this region of pVHL forms a helix that fits into a concave surface present on elongin C [35]. It seems likely that inhibition of elongin A contributes to pVHL function, and this competition between VHL156-171 and elongin A may be related to the effect of the peptide on neuronal differentiation of NPCs.

In conclusion, here we showed the neuronal differentiation of NPCs elicited by the intracellular delivery of a synthetic oligopeptide composed of 16 amino acids derived from pVHL. This finding provides a novel approach for the regulation of cellular differentiation of NPCs.

REFERENCES

[1] Dharap, S.S.; Chandna, P., Wang; Y., Khandare, J.J.; Qiu, B., Stein, S.; Minko, T. Molecular targeting of BCL2 and BCLXL proteins by synthetic BCL2 homology 3 domain peptide enhances the efficacy of chemotherapy. J. Pharmacol. Exp. Ther., **2006**, *316*(3), 992-928.

[2] Do, T.N.; Rosal, R.V.; Drew, L.; Raffo; A.J.; Michl, J.; Pincus, M.R.; Friedman, F.K.; Petrylak, D.P.; Cassai, N.; Szmulewicz, J.; Sidhu, G.; Fine, R.L.; Brandt-Rauf, P.W. Preferential induction of necrosis in human breast cancer cells by a p53 peptide derived from the MDM2 binding site. *Oncogene*, **2003**, *22*(10), 1431-1444.

[3] Korzick, D.H.; Kostyak, J.C.; Hunter, J.C.; Saupe, K.W. Local delivery of PKCepsilon-activating peptide mimics ischemic preconditioning in aged hearts through GSK-3beta but not F1-ATPase inactivation. *Am. J. Physiol. Heart. Circ. Physiol.*, **2007**, *293*(4), H2056-2063.

[4] Pudi, R.; Ramamurthy, S.S.; Das, S. A peptide derived from RNA recognition motif 2 of human la protein binds to hepatitis C virus internal ribosome entry site, prevents ribosomal assembly, and inhibits internal initiation of translation. *J. Virol.*, **2005**, *79*(15), 9842-9853.

[5] Lavaur, J.; Bernard, F.; Trifilieff, P.; Pascoli, V.; Kappes, V.; Pagès, C.; Vanhoutte, P.; Caboche, J. *J. Neurosci.*, **2007**, *27*(52), 14448-14458.

[6] Gil, G.A.; Bussolino, D.F.; Portal, M.M.; Pecchio, A.A.; Renner, M.L.; Borioli, G.A.; Guido, M.E.; Caputto, B.L. c-Fos activated phospholipid synthesis is required for neurite elongation in differentiating PC12 cells. *Mol. Biol. Cell*, **2004**, *15*(4), 1881-1894.

[7] Anestål, K.; Arnér, E.S. Rapid induction of cell death by selenium-compromised thioredoxin reductase 1 but not by the fully active enzyme containing selenocysteine. *J. Biol. Chem.*, **2003**, *278*(18), 15966-15972.

[8] Bradley, C.K.; Takano, E.A.; Hall, M.A.; Göthert, J.R.; Harvey, A.R.; Begley, C.G.; van Eekelen, J.A. The essential haematopoietic transcription factor Scl is also critical for neuronal development. *Eur. J. Neurosci.*, **2006**, *23*(7), 1677-1689.

[9] Wang, L.; Zhang, Z.G.; Zhang, R.L.; Jiao, Z.X.; Wang, Y.; Pourabdollah-Nejad, D. S.; Le Tourneau, Y.; Gregg, S.R.; Chopp, M. Neurogenin 1 mediates erythropoietin enhanced differentiation of adult neural progenitor cells. *J. Cereb. Blood. Flow. Metab.*, **2006**, *26*(4), 556-564.

[10] Horton, S.; Meredith, A.; Richardson, J.A.; Johnson, J.E. Correct coordination of neuronal differentiation events in ventral forebrain requires the bHLH factor MASH1. *Mol. Cell. Neurosci.*, **1999**, *14*(4-5), 355-369.

[11] Shin, M. H.; Lee, E.G.; Lee, S.H.; Lee, Y.S.; Son, H. Neural cell adhesion molecule (NCAM) promotes the differentiation of hippocampal precursor cells to a neuronal lineage, especially to a glutamatergic neural cell type. *Exp. Mol. Med.*, **2002**, *34*(6), 401-410.

[12] Ito, H.; Nakajima, A.; Nomoto, H.; Furukawa, S. Neurotrophins facilitate neuronal differentiation of cultured neural stem cells via induction of mRNA expression of basic helix-loop-helix transcription factors Mash1 and Math1. *J. Neurosci. Res.*, **2003**, *71*(5), 648-

658.

[13] Ahmed, S.; Reynolds, B.A.; Weiss, S. BDNF enhances the differentiation but not the survival of CNS stem cell-derived neuronal precursors. *J. Neurosci.*, **1995**, *15*(8), 5765-5778.

[14] Arsenijevic, Y.; Weiss, S. Insulin-like growth factor-I is a differentiation factor for postmitotic CNS stem cell-derived neuronal precursors: distinct actions from those of brain-derived neurotrophic factor. *J. Neurosci.*, **1998**, *18*(6), 2118-2128.

[15] Galli, R.; Pagano, S.F.; Gritti, A.; Vescovi, A.L. Regulation of neuronal differentiation in human CNS stem cell progeny by leukemia inhibitory factor. *Dev. Neurosci.*, **2000**, *22*(1-2), 86-95.

[16] Kitayama, T.; Yoneyama, M.; Tamaki, K.; Yoneda,Y. Regulation of neuronal differentiation by N-methyl-D-aspartate receptors expressed in neural progenitor cells isolated from adult mouse hippocampus. *J. Neurosci. Res.*, **2004**, *76*(5), 599-612.

[17] Liste, I.; García-García, E.; Martínez-Serrano, A. The generation of dopaminergic neurons by human neural stem cells is enhanced by Bcl-XL, both *in vitro* and *in vivo*. *J Neurosci.*, **2004**, *24*(48), 10786-10795.

[18] Dutton, R.; Yamada, T.; Turnley, A.; Bartlett, P.F.; Murphy, M. Sonic hedgehog promotes neuronal differentiation of murine spinal cord precursors and collaborates with neurotrophin 3 to induce Islet-1. *J. Neurosci.*, **1999**, *19*(7), 2601-2608.

[19] Kim, T.E.; Lee, H.S.; Lee, Y.B.; Hong, S.H.; Lee, Y.S.; Ichinose, H.; Kim, S.U.; Lee, M.A. Sonic hedgehog and FGF8 collaborate to induce dopaminergic phenotypes in the Nurr1-overexpressing neural stem cell. *Biochem. Biophys. Res. Commun.*, **2003**, *305*(4), 1040-1048.

[20] Wagner, J.; Akerud, P.; Castro, D.S.; Holm, P.C.; Canals, J.M.; Snyder, E.Y.; Perlmann, T.; Arenas, E. Induction of a midbrain dopaminergic phenotype in Nurr1-overexpressing neural stem cells by type 1 astrocytes. *Nat. Biotechnol.*, **1999**, *17*(7), 653-659.

[21] Pevny, L.H.; Sockanathan, S.; Placzek, M.; Lovell-Badge, R. A role for SOX1 in neural determination. *Development*, **1998**, *125*(10), 1967-1978.

[22] Uittenbogaard, M.; Chiaramello, A. Expression of the bHLH transcription factor Tcf12 (ME1) gene is linked to the expansion of precursor cell populations during neurogenesis. *Brain Res. Gene Expr. Patterns*, **2002**, *1*(2), 115-121.

[23] Kanno, H.; Saljooque, F.; Yamamoto, I.; Hattori, S.; Yao, M.; Shuin, T; U, H.S. Role of the von Hippel-Lindau tumor suppressor protein during neuronal differentiation. *Cancer Res.*, **2000**, *60*(11), 2820-2824.

[24] Link, C.J.Jr; Kolb, E.M.; Muldoon, R.R. *Hybridoma*, **1995**, *14*(2), 143-147.

[25] Powell, S.K.; Kaloss, M.; Burimski, I.; Weaver, L.; Long, Z.; Lyons, R.; McGarrity, G.J.; Otto, E. *In vitro* analysis of transformation potential associated with retroviral vector insertions. *Hum. Gene Ther.*, **1999**, *10*(13), 2123-2132.

[26] Conrad, C.; Gupta, R.; Mohan, H.; Niess, H.; Bruns, C.J.; Kopp, R.; von Luettichau, I.; Guba, M.; Heeschen, C.; Jauch, K.W.; Huss, R.; Nelson, P.J. *Curr. Gene Ther.*, **2007**, *7*(4), 249-260.

[27] Spitere, K.; Toulouse, A.; O'Sullivan, D.B.; Sullivan, A.M. TAT-PAX6 protein transduction in neural progenitor cells: a novel approach for generation of dopaminergic neurones *in vitro*. *Brain Res.*, **2008**, *1280*, 25-34.

[28] Stebbins, C. E.; Kaelin, W. G., Jr.; Pavletich, N. P. Structure of the VHL-ElonginC-ElonginB complex: implications for VHL tumor suppressor function. *Science*, **1999**, *284*(5413), 455-461.

[29] Ohh, M.; Takagi, Y.; Aso, T.; Stebbins, C.E.; Pavletich, N.P.; Zbar, B.; Conaway, R.C.; Conaway, J.W.; Kaelin, W.G. Jr. Synthetic peptides define critical contacts between elongin C, elongin B, and the von Hippel-Lindau protein. *J. Clin. Invest.*, **1999**, *104*(11), 1583-1591.

[30] Iwai, K.; Yamanaka, K.; Kamura, T.; Minato, N.; Conaway, R. C.; Conaway, J.W.; Klausner, R.D.; Pause, A. Identification of the von Hippel-Lindau tumor-suppressor protein as part of an active E3 ubiquitin ligase complex. *Proc. Natl. Acad. Sci. USA*, **1999**, *96*(22), 12436-12441.

[31] Bryan, B.; Cai, Y.; Wrighton, K.; Wu, G.; Feng, X.H.; Liu, M. Ubiquitination of RhoA by Smurf1 promotes neurite outgrowth. *FEBS Lett.*, **2005**, *579*(5), 1015-1019.

[32] Smith-Thomas, L.C.; Kent, C.; Mayer, R.J.; Scotting, P.J. Protein ubiquitination and neuronal differentiation in chick embryos. *Brain Res. Dev. Brain Res.*, **1994**, *81(2)*, 171-177.

[33] Coulombe, P.; Rodier, G.; Pelletier, S.; Pellerin, J.; Meloche, S. Rapid turnover of extracellular signal-regulated kinase 3 by the ubiquitin-proteasome pathway defines a novel paradigm of mitogen-activated protein kinase regulation during cellular differentiation. *Mol. Cell. Biol.*, **2003**, *23*(13), 4542-4558.

[34] Spencer, M.L.; Theodosiou, M.; Noonan, D.J. NPDC-1, a novel regulator of neuronal proliferation, is degraded by the ubiquitin/proteasome system through a PEST degradation motif. *J. Biol. Chem.*, **2004**, *279*(35), 37069-37078.

[35] Bai, S.; Datta, J.; Jacob, S.T.; Ghoshal, K. Treatment of PC12 cells with nerve growth factor induces proteasomal degradation of T-cadherin that requires tyrosine phosphorylation of its cadherin domain. *J. Biol. Chem.*, **2007**, *282*(37), 27171-27180.

[36] Botuyan, M.V.; Mer, G.; Yi, G.S.; Koth, C.M.; Case, D.A.; Edwards, A.M.; Chazin, W.J.; Arrowsmith, C.H. Solution structure and dynamics of yeast elongin C in complex with a von Hippel-Lindau peptide. *J. Mol. Biol.*, **2001**, *312*(1), 177-186.

[37] Yamada, H.; Dezawa, M.; Shimazu, S.; Baba, M.; Sawada, H.; Kuroiwa, Y.; Yamamoto, I.; Kanno, H. Transfer of the von Hippel-Lindau tumor suppressor gene to neuronal progenitor cells in treatment for Parkinson's disease. *Ann. Neurol.*, **2003**, *54*(3), 352-359.

[38] Murata, H.; Tajima, N.; Nagashima, Y.; Yao, M.; Baba, M.; Goto, M.; Kawamoto, S.; Yamamoto, I.; Okuda, K.; Kanno, H. Von Hippel-Lindau Tumor Suppressor Protein Transforms Human Neuroblastoma Cells into Functional Neuron-like Cells. *Cancer Res.*, **2002**, *62*(23), 7004-7011.

[39] Zelphati, O.; Wang, Y.; Kitada, S.; Reed, J.C.; Felgner, P.L.; Corbeil, J. Intracellular delivery of proteins with a new lipid-mediated delivery system. *J. Biol. Chem.*, **2001**, *276*(37), 35103-35110.

[40] Zheng, X.; Lundberg, M.; Karlsson, A.; Johansson, M. Lipid-mediated protein delivery of suicide nucleoside kinases. *Cancer Res.*, **2003**, *63*(20), 6909-6913.

[41] Schwarze, S. R.; Ho, A.; Vocero-Akbani, A.; Dowdy, S. F. *In vivo* protein transduction: delivery of a biologically active protein into the mouse. *Science*, **1999**, *285*(5433), 1569-1572.

[41] Perez, F., Joliot, A. H., Bloch-Gallego, E., Zahraoui, A., Triller, A., and Prochiantz, A. Antennapedia homeobox as a signal for the cellular internalization and nuclear addressing of a small exogenous peptide. *J. Cell Sci.*, **1992**, *102*(4), 717-.722

Received: August 11, 2008 **Revised: October 02, 2008** **Accepted: October 03, 2008**

INVITED REVIEW ARTICLE

Nagoya J. Med. Sci. 71. 101 ~ 107. 2009

ADVANCED NEW NEUROSURGICAL PROCEDURE USING INTEGRATED SYSTEM OF INTRAOPERATIVE MRI AND NEURONAVIGATION WITH MULTIMODAL NEURORADIOLOGICAL IMAGES

TOSHIHIKO WAKABAYASHI, MASAZUMI FUJII, YASUKAZU KAJITA, ATSUSHI NATSUME, SATOSHI MAEZAWA and JUN YOSHIDA

Department of Neurosurgery, Nagoya University Graduate School of Medicine

ABSTRACT

The purpose of this paper is to describe the newly-established technique in the field of neurological surgery for fusion imaging of three-dimensional magnetic resonance image (3D-MRI) and/or three-dimensional computed tomography (3D-CT) for brain tumor surgery. Combining neuronavigation technology and intraoperative MRI, this method remarkably demonstrates spatial relationships of neurovascular structures and/or skull base landmarks and is very useful for intraoperative evaluation of completed neurosurgical operations. Using the navigation system and intraoperative MRI during surgery, it is possible to resect the brain tumor maximally and preserve essential neurological functions. Furthermore, advanced multimodal neuroradiological images such as functional MRI (fMRI), diffusion tensor imaging (DTI), MR spectroscopy (MRS), and positron emission tomography (PET) clearly demonstrate the dominant cortex including the speech center, primary motor gyrus, primary sensory gyrus, and support high-quality operation with less invasive surgery. In conclusion, multimodal neuroradiological images are very useful for invasive non-circumscribed brain tumors such as glioma and, in combination with such highly technological analyses, advanced neurosurgical procedures are possible.

Key Words: Intraoperative MRI, Fusion image, Three-dimensional image, Glioma, Neuronavigation

INTRODUCTION

Recent promotion of collaboration between medical science and engineering has brought about significant advancement in the development of diagnostic imaging technology and surgical assisted systems.[1] Using a high-resolution microscope, the operation requires high-accuracy technique that refers to the 3D brain image displayed on the neuronavigation robot within a close tolerance of a few millimeters; it is reminiscent of repairs made to a sophisticated electronic circuit.[2] On the other hand, the advancement of computer technology makes 3D virtual image technology more efficient, allowing the creation of images analogous to the clinical condition. As a result, it is becoming possible to establish a correct diagnosis of a minute lesion.[3] Moreover, "brain shift," the greatest weakness of a neuronavigative operation, was resolved at once due to the development of image fusion technology which utilizes intraoperative MRI images for visualization of changes

Corresponding author: Toshihiko Wakabayashi

Department of Neurosurgery, Nagoya University Graduate School of Medicine,

65 Tsurumai-cho, Showa-ku, Nagoya 466-8550, Japan

Phone: +81-52-744-2355, Fax: +81-52-744-2361, E-mail: wakabat@med.nagoya-u.ac.jp

in brain morphology so that the navigation map can be adjusted during the surgical procedure. In a neurosurgical operation, this information integration among image, organ and function assures a good balance between maximum tumor resection for overall survival prognosis and provides a functional prognosis even for invasive malignant brain tumors[4]. Furthermore, this innovation provides the momentum for development of surgical devices applicable even in the microscopic field[5]. At present, the Department of Neurosurgery, Nagoya University Graduate School of Medicine is working on a project for "development of an intelligent operation system" along with the Department of Mechanical Engineering, Nagoya Institute of Technology and Department of Media Science, Nagoya University Graduate School of Technology. The goal of the project is to create the world's first intraoperative brain touch sensor and/or microsurgical device for microscopic or endoscopic management.[6]

"Brain Theater," the integrated system of intraoperative MRI and neuronavigation, was set up at Nagoya University Hospital in January of 2006 (Fig. 1). The system features new technology which provides surgical assistance information gathered through intraoperative MRI and networks not only for the operation theater but to other universities and hospitals as well. Briefly, the system works as follows: 1) as a core function, an MRI (Hitachi) is situated at No. 5 operation theater at Nagoya University Hospital. 2) An intraoperative neuronavigation system functions in perfect unison with the operative microscope and peripheral equipment. 3) The secure and high-performance operation theater encourages neurosurgeons to make full use of traditional surgical techniques without qualification (Fig. 2). 4) Awarded the 2007 good design award from the Japan Industrial Design Promotion Organization. Additionally, by making this available on line, it is possible to share the surgical assist

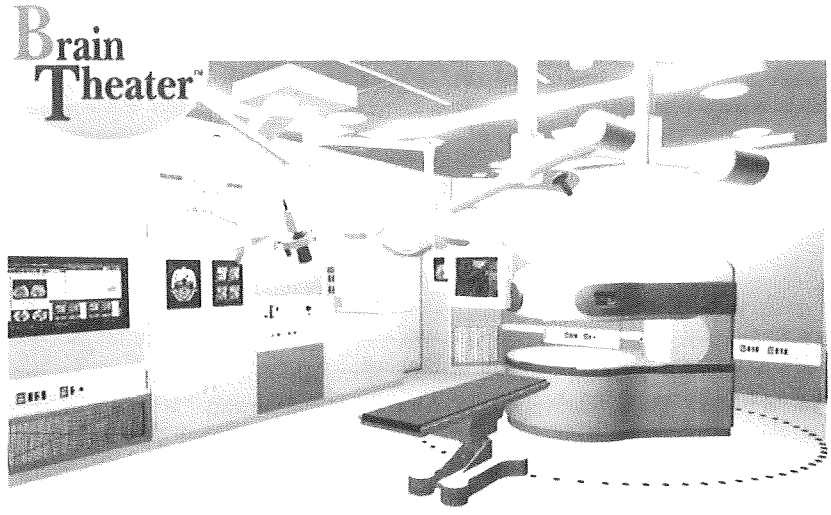

Fig. 1 Neurosurgical operation room No. 5 called the "Brain Theater," equipped with open MRI unit (0.4 Tesla HITACHI Aperto) at Nagoya University Hospital. (Low magnetic field and rotation table concept; 1) safer, 2) standard-equipped with all conventional systems, 3) applicable to non-MRI operation, 4) permanent magnet with lower cost (primary as well as running cost), 5) specially designed table for easy patient transportation to scanner, and 6) sufficient image quality).

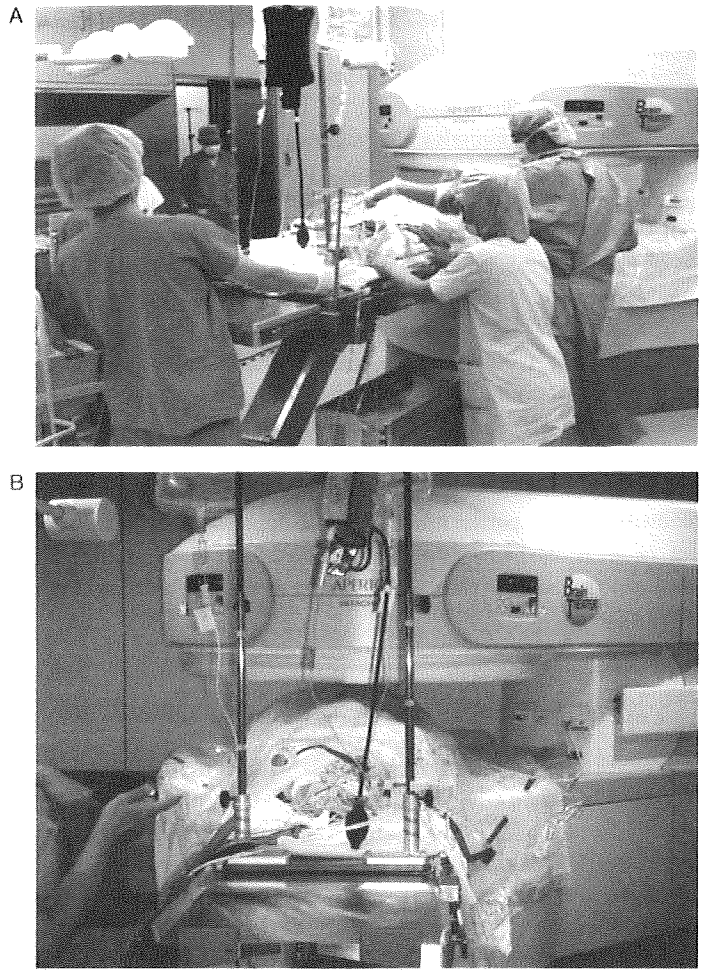

Fig. 2 Setup position for intraoperative MRI during neurological surgery in Brain Theater.
A: Transportation of patient to setup. B: Setup position of patient in intraoperative MRI.

system for surgical planning, sharing intraoperative images, supporting tele-surgery, and developing advanced therapy outside the operation theater. With the great technical assistance of the Graduate School of Information Science, Nagoya University and the Department of Radiological Technology, Nagoya University School of Health Science, the system can develop educational and training activities for students and young neurosurgeons in terms of surgical simulation before an operation. Besides, the simulated experience of operations produced by sharing virtual images is useful to decide the strategy for clinical cases.

In 2007, the "brain SUITE," operation assistance equipment, similar to the "Brain Theater" made by Siemens, was installed at Nagoya Central Hospital in connection with the relocation of the hospital. Since it is a Nagoya University-affiliated hospital, these two systems are linked by network to exchange information so that it is now possible to assist with difficult operations mutually by remote control. It is easy to imagine that the surgical assist system brought about by 3D virtual images will show rapid progress hand in hand with the advancement of image analysis.

PROGRESS IN DIAGNOSTIC IMAGING IN THE FIELD OF NEUROSURGERY

Progress in neurosurgical diagnostics is supported by advancements in diagnostic radiology imaging. Along with advancements in diagnostic radiology, various kinds of neuroimaging are produced which are useful for preoperative diagnosis, planning operation strategy, intraoperative image assistance, and postoperative follow-up. As for MRI scans, not only standard models such as T1 weighted-image, T2 weighted-image and FLAIR images but also the emergence of new models with diffusion-weighted image, ADC (Apparent Diffusion Coefficient) MAP, MR Angiography have increased the range of qualitative diagnosis and are already used in clinical settings. Such evolution foretells the near future when tissue diagnosis can be done merely by image analysis. In addition, PET as typified by FDG-PET, radionuclide scanning (e.g. SPECT), and magnetic encephalography have made qualitative diagnosis possible.[7] Besides, nowadays X-ray computed tomography can be treated as a 3D image since multislice helical CT has become increasingly more widespread. The use of these various technologies for preoperative evaluation and intraoperative assistance has made more accurate neurosurgery feasible. Moreover, progress in computer technology makes it possible to utilize advanced 3D virtual images for more advanced image analysis.[8] In particular, the Graduate School of Information Science, Nagoya University (Chief of projects: Dr. Kensaku Mori, PhD, Main Assistance: Dr. Yu-ichiro Hayashi, PhD) has designed the fastest software for image analysis and collaborative research is expected to deliver optimum results.

PROGRESS IN NEUROSURGICAL OPERATION

Neurosurgery has made steady progress, thanks to the introduction of microsurgery in the 1960s, the development of micro-operative devices in the 1970s, the spread of the head computed tomography scans in the 1980s, and the significant improvement of diagnostic techniques provided by the spread of MRI in the 1990s. Meanwhile, it is also obvious that continuous efforts by neurosurgeons have resulted in excellent progress. Brain tumors, particularly in infiltrative intraparenchymal tumors such as glioma, require delicate surgery; however, wide tumor resection might cause brain dysfunction and/or an adverse effect. Therefore, an immediate decision based on both improved resection and avoidance of dysfunction is necessary. Consequently, for the

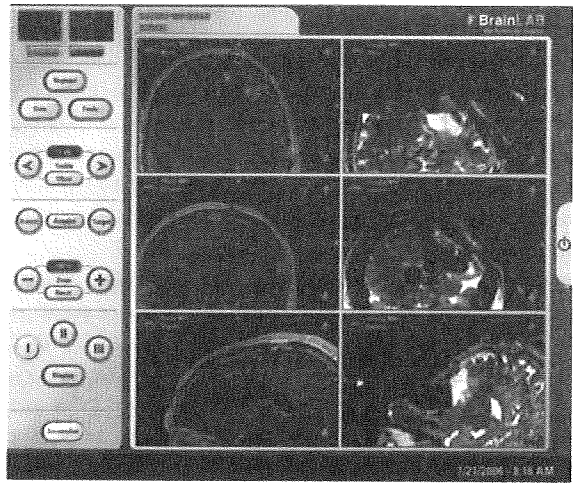

Fig. 3 Comparison of MRI image on neuronavigation display (Left: preoperative axial, coronal, and sagittal views on T1WI. Right: intraoperative axial, coronal, and sagittal view on T2WI). Note remarkable "brain shift" after connection of ventricle with tumor removal cavity.

Table 1 Profile of 18 recent operative cases of glioma performed in Brain Theater. Remarkably improved removal rate of tumor on postoperative MRI was achieved. (GBM: glioblastoma multiforme; CN: central neurocytoma; O: oligodendroglioma; AO: anaplastic oligodendroglioma; A: astrocytoma)

Case	Age	M/F	Histology	Location	Tumor size (ml)	MRI sequence	Resection rate (%)	neurology (postop.)
1	20	F	GBM	rt Th	60.1	T1 (E)	93.9	Gerstmansyndrome
2	20	M	CN	rt LV	49.5	T1 (E)	100.0	free
3	29	F	O	rt F	81.9	T2	83.4	free
4	58	M	GBM	rt F, M	20.3	T1 (E)	100.0	no change
5	30	M	AO	lt T	180.5	FL	100.0	free
6	56	M	AO	lt T	71.2	T1 (E)	100.0	no change
7	67	F	GBM	rt T	12.1	T1 (E)	100.0	free
8	38	F	A	rt Ol	51.5	T1 (E)	100.0	no change
9	31	M	O	lt F	69.1	T1 (P)	100.0	improved
10	72	M	A	lt F	25.7	T2	94.3	transient aphasia
11	56	F	GBM	rt P	91.2	T1 (E)	100.0	free
12	40	M	A	lt F	55.3	T2	85.9	transient aphasia
13	55	M	O	lt P	71.5	T2	90.3	transient aphasia
14	61	F	O	rt F	31.5	T2	80.9	free
15	66	M	GBM	lt F	87.4	T1 (E)	97.7	no change
16	60	M	O	rt F	23.8	T1 (E)	95.5	no change
17	66	M	GBM	rt P	10.8	T1 (E)	100.0	no change
18	50	M	AO	rt F	3.9	T1 (E)	100.0	no change
MEAN	48.6				55.4		95.7	

success of these surgical procedures involving tumors, it is essential to combine them with image-guided surgery, a technique based on neuronavigation which first introduced in the 1990s.

The neuronavigation system is a useful surgical-assisted device which can provide accurate information on the surgical site in real time. However, existing navigation functioned based on preoperative imaging has inherent fundamental problems involving the "brain shift." It means change in the shape of the brain during an operation.[9] For example, during surgical procedures, the removal of a space-occupying lesion or drainage of cerebrospinal fluid often causes distortion so that the brain surface sinks several centimeters (Fig. 3). Since this change in brain shape undermines the reliability of navigation which uses a preoperative image as a map, the appropriate adjustment for such brain shifts has become an urgent necessity. In response, using intraoperative MRI to confirm changes in brain morphology, image fusion technology enables a navigation system to adjust the images during an operation so as to resolve the problem (Table 1). Although

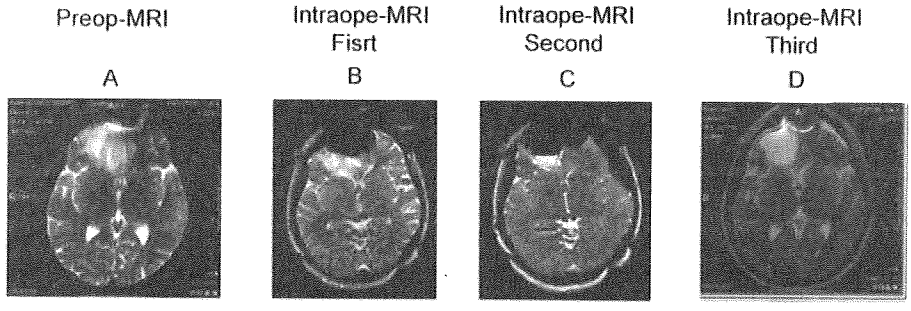

Fig. 4 Illustrative case of right frontal oligodendroglioma, primary case. A: Pre-operative MRI (T2 weighted image) before surgery revealed a relatively huge mass at the entire right frontal tip invading the corpus callusum at the bottom of this mass. B: Intraoperative MRI during surgery showed a residual tumor at the bottom of this removal cavity. C: Second intraoperative MRI revealed subtotal removal with still small residual mass at the bottom of this cavity. D: Third intraoperative MRI eventually showed total removal of this mass.

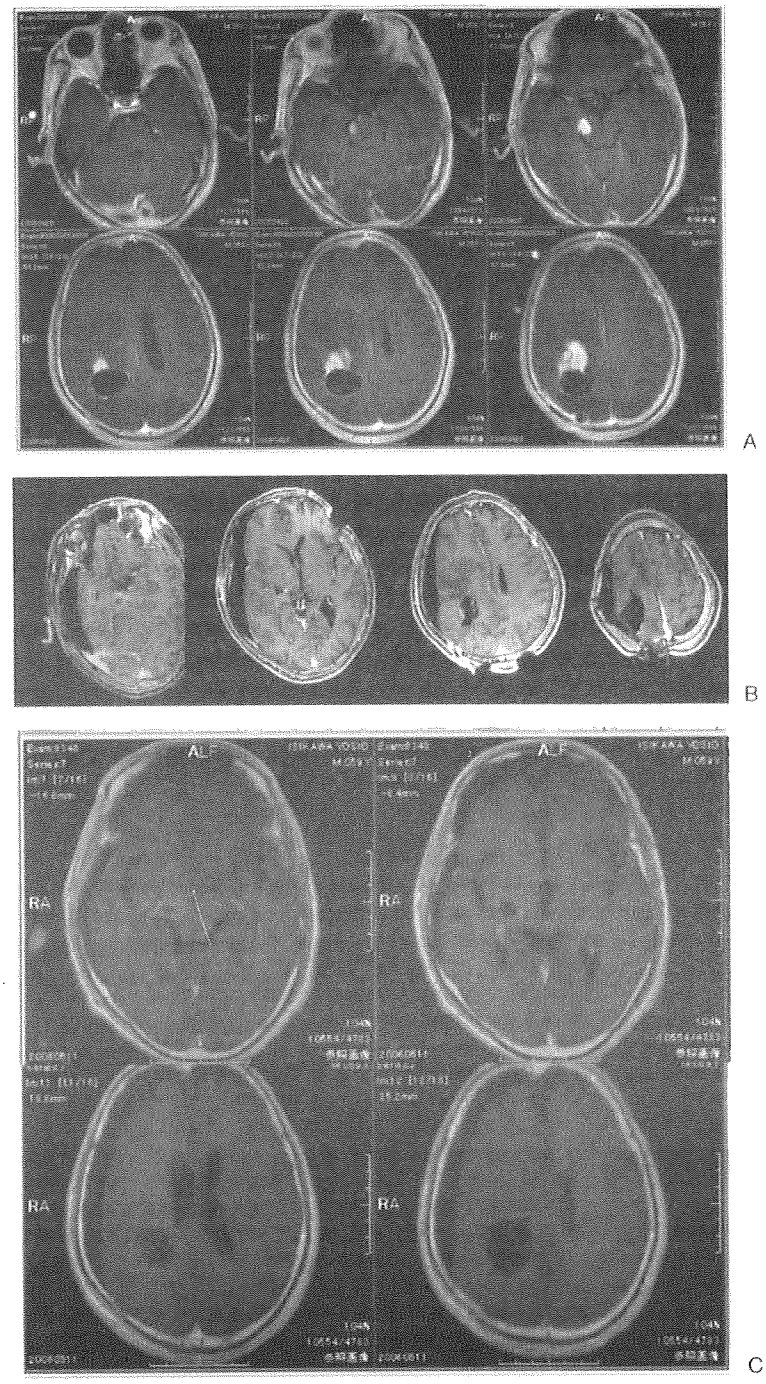

Fig. 5 Illustrative case of recurrent glioblastoma occurring primarily at right parietal site. A: Pre-operative MRI (T1WI gadolinium enhanced axial image) revealed multiple recurrent enhanced masses not only in adjacent area of pre-operative space but also in remote area as a part of midbrain. B: Intraoperative MRI during surgery showed removal of almost all mass with a small residual tumor at part of the remote disseminated area on midbrain. C: Final intraoperative MRI indicated complete removal of mass.

the advancement in imaging technology is significant, the images of brain function are still not completely reliable; therefore, physiological monitoring such as SEP, MEP and ABP should be used in combination in order to achieve operation safety.[10] Also, with tumors near the language area, intraoperative brain function monitoring under awake craniotomy is considered important. Tumor resection is the most important target in future neurosurgical operations. Three kinds of information, image, organ, and function, should be integrated to balance competing goals for maximum resection and ensuring safety (Fig. 4 and Fig. 5).

FUTURE PROGRESS IN NEUROSURGERY

To achieve minimally invasive and accurate neurosurgical operations, the development of more sophisticated diagnostic devices and surgical-assist devices is required. Present advances in prevention medicine enhance the opportunities for early detection by brain medical checkups and rapid cures of neurosurgical disorders, that might otherwise cause serious disability. Now we are at a major turning point for neurosurgical treatment since safer and more secure ways of providing it have been established as prevention measures in recent years. Now there is a pressing need to create a support system by promoting expertise and innovations to meet the increasing demand for neurosurgical treatment.[11]

In conclusion, multimodal neuroradiological images are very useful for invasive non-circumscribed brain tumors such as glioma and further progress in the field of medical technology may bring about a next-generation neurosurgical world.

REFERENCES

1) Darakchiev BJ, Tew JM Jr, Bohinski RJ, Warhick RE. Adaptation of a standard low-field (0.3-T) system to the operating room: focus on pituitary adenomas. *Neurosurg Clin N Am*, 2005; 16: 155–164.
2) Fahlbusch R, Ganslandt O, Buchfelder M, Schott W, Nimnsky C. Intraoperative magnetic resonance imaging during transsphenoidal surgery. *J Neurosurg*, 2001; 95: 381–390.
3) Kelly JJ, Hader WJ, Myles ST, Sutherland GR. Epilepsy surgery with intraoperative MRI at 1.5 T. *Neurosurg Clin N Am*, 2005; 16: 173–183.
4) Matsumae M, Koizumi J, Fukuyama H, Ishizaka H, Mizokami Y, Baba T, Atsumi H, Tsugu A, Oda S, Tanaka Y, Osada T, Imai M, Ishiguro T, Yamamoto M, Tominaga J, Shimoda M, Imai Y. World's first magnetic resonance imaging/X-ray/operating room suite: a significant milestone in the improvement of neurosurgical diagnosis and treatment. *J Neurosurg*, 2007; 107: 266–273.
5) Nimnsky C, Ganslandt O, Fahlbusch R. 1.5-T intraoperative imaging beyond standard anatomic imaging. *Neurosurg Clin N Am*, 2005; 16: 185–200.
6) Oh DS, Black PM. A low-field intraoperative MRI system for glioma surgery: is it worthwhile? *Neurosurg Clin N Am*, 2005; 16: 105–114.
7) Schulder M, Catrambone J, Carmel PW. Intraoperative magnetic resonance imaging at 0.12 T. Is it enough? *Neurosurg Clin N Am*, 2005; 16: 143–154.
8) Bello L, Gambini A, Castellano A. Motor and language DTI fiber tracking combied with intraoperative subcortical mapping for surgical removal of gliomas. *Neuro-image*, 2008; 39: 369–382.
9) Bermann JI, Berger MS, Chung SW. Accuracy of diffusion tensor magnetic resonance imaging tractography assessed using intraoperative subcortical stimulation mapping and magnetic source imaging. *J Neurosurg*, 2007; 107: 488–494.
10) Roessler K, Gatterbauer B, Becherer A. Surgical target selection in cerebral glioma surgery: linking methionine (MET) PET image fusion and neuronvigation. *Minim Invasive Neurosurg*, 2007; 50: 273–280.
11) Tanaka Y, Nariai T, Momose T. Glioma surgery using a multimodal navigation system with integrated metabolic images. *J Neurosurg*, 2009; 110: 163–172.

Published Online First on November 24, 2009

The Modulation of MicroRNAs by Type I IFN through the Activation of Signal Transducers and Activators of Transcription 3 in Human Glioma

Masasuke Ohno,[1] Atsushi Natsume,[1,2] Yutaka Kondo,[3] Hidetaka Iwamizu,[1] Kazuya Motomura,[1] Hiroshi Toda,[1] Motokazu Ito,[1,2] Takenori Kato,[1] and Toshihiko Wakabayashi[1]

[1]Department of Neurosurgery, [2]Center for Genetic and Regenerative Medicine, Nagoya University School of Medicine, and [3]Division of Molecular Oncology, Aichi Cancer Center Research Institute, Nagoya, Japan

Abstract

Type I IFNs are involved in double-stranded RNA responses. Here, we investigated the possibility that IFN-β may induce or downregulate cellular microRNAs (miRNA) in human neoplasms and thereby use the RNA interference system to show antitumor effects. Because of its known connection to glioma biology, we focused on miR-21 among seven miRNAs influenced by IFN-β. We analyzed the effect of IFN-β treatment on miR-21 expression in glioma cells and intracranial glioma xenografts. IFN-β treatment reduced miR-21 expression in glioma cells markedly, and IFN-β administration suppressed the growth of glioma-initiating cell–derived intracranial tumors. The levels of primary *miR-21* gene transcripts, precursor miR-21, and mature miR-21 decreased 6 hours after the addition of IFN-β, indicating that the reduction in miR-21 levels was due to transcriptional suppression. We did reporter assays to elucidate the IFN-β–mediated suppression of miR-21; the addition of signal transducers and activators of transcription 3 (STAT3)–expressing vectors induced the IFN-β–mediated suppression of miR-21, whereas STAT3-inhibiting agents inhibited the miR-21 suppression. Thus, the results of our study show that the downregulation of miR-21 contributes to the antitumor effects of IFN-β and that miR-21 expression is negatively regulated by STAT3 activation. These results highlight the importance of understanding the transcriptional regulation of the miRNAs involved in oncogenesis. (Mol Cancer Res 2009;7(12):OF1–9)

Introduction

MicroRNAs (miRNA) are small noncoding RNAs consisting of 20 to 22 nucleotides that participate in the posttranslational regulation of gene expression by means of RNA interference (RNAi). The miRNA genes are transcribed by RNA polymerase II in the nucleus to form large pri-miRNA transcripts. These pri-miRNA transcripts are processed by Drosha to release the pre-miRNA precursor product, which is less than 70 nucleotides in length. After the pre-miRNA is transported into the cytoplasm, Dicer processes the intermediate to generate a mature 22-nucleotide miRNA. This mature miRNA is integrated into the RNA-induced silencing complex (1) and forms double-stranded RNA with complementary mRNAs (mRNA). Depending on the degree of homology between the miRNA and the mRNA, the RNA-induced silencing complex could inhibit mRNA function by either promoting its cleavage or by inhibiting its translation (2, 3). Emerging evidence suggests that miRNAs are involved in crucial biological processes, including the development, differentiation, apoptosis, and proliferation of mammalian cells (4). In humans, miRNAs have been proposed to contribute to oncogenesis because they possess multifaceted functions either as tumor suppressors or as oncogenes (5).

RNA interference induces a multitude of responses in addition to the knockdown of a gene. This is best understood in the context of an antiviral immune response. In particular, double-stranded RNA, a nucleic acid associated with viral replication, is involved in numerous interactions contributing to the induction, activation, and regulation of antiviral mechanisms. It is especially responsible for stimulating important protective responses such as the activation of dicer-related antiviral pathways, induction of type I IFN (IFN-α/β), and stimulation of double-stranded RNA–activated protein kinase and oligoadenylate synthase (6). IFN-α/β regulates the levels of crucial mediators of the antiviral response, such as protein kinase R, the 2′-5′ oligoadenylate synthase/RNase L system, the adenosine deaminase ADR1, or the Mx GTPase (7, 8). Thus, RNA interference might be involved in the IFN-mediated antiviral response. It was recently reported that the levels of liver-specific miRNA, i.e., miR-122, and several other miRNAs are regulated by IFN-β in human hepatoma cells, and that IFN-β rapidly modulates the expression of miRNAs, which target the hepatitis C virus genomic RNA, and thus, inhibits viral replication (9, 10).

In addition to its ability to interfere with viral replication, IFN-β is also known for its antiproliferative effects in a variety of neoplasms such as hepatocellular carcinoma, chronic myeloblastic leukemia, melanoma, renal cancer, and glioma (11, 12). However, the possibility that IFN-β might induce or downregulate cellular miRNAs in human neoplasms and thereby use the RNA interference system in its action against tumor progression has been left unexplored.

Received 7/22/09; revised 10/10/09; accepted 10/14/09; published OnlineFirst 11/24/09.
The costs of publication of this article were defrayed in part by the payment of page charges. This article must therefore be hereby marked *advertisement* in accordance with 18 U.S.C. Section 1734 solely to indicate this fact.
Note: Supplementary data for this article are available at Molecular Cancer Research Online (http://mcr.aacrjournals.org/).
Requests for reprints: Atsushi Natsume, Department of Neurosurgery, Center for Genetic and Regenerative Medicine, Nagoya University School of Medicine, Nagoya 466-8550, Japan. Phone: 81-52-744-2353; Fax: 81-52-744-2360. E-mail: anatsume@med.nagoya-u.ac.jp

doi:10.1158/1541-7786.MCR-09-0319

Malignant glioma represents ~20% of all intracranial tumors. Despite the advances in radiation therapy and chemotherapy administered after the surgical resection of the tumor, the prognosis of malignant glioma remains poor, with a median survival time of <10 months (13). In the treatment of malignant gliomas, IFN-β exhibits pleiotropic biological effects such as antiproliferation, immunomodulation, induction of differentiation from glioma-initiating cells (GIC), and drug sensitization by classically activating Janus kinase/signal transducers and activators of transcription (STAT) pathways (14, 15). However, there is no report on IFN-mediated modulation of cellular miRNAs as an antitumor mechanism.

In the present study, we test whether IFN-β can alter the expression of cellular miRNAs in human glioma cells by using the data obtained from genomewide microarray technology. On the basis of the initial screening efforts identifying several increased or attenuated miRNAs, we show that in cultured glioma cells and orthotopic glioma xenograft, IFN-β treatment leads to STAT3-mediated reduction in the expression of miR-21, an antiapoptotic miRNA that has been shown to be overexpressed in gliomas (16).

Results

Differential miRNA Expression in Human Glioma Cells Treated with IFN-β

To investigate which miRNAs are induced or downregulated by IFN-β, we used a microarray containing 662 mammalian miRNAs. We identified a total of two overexpressing and five underexpressing human miRNAs in the IFN-β–treated glioma cells. The expression of miRNAs, including miR-187 and miR-194, was increased >2-fold, whereas that of miR-100, let-7a, let-7b, let-7c, and miR-21 was decreased <0.5-fold in the T98 cell line treated with IFN-β as compared with the expression levels in cells without any treatment (Fig. 1A; Supplementary Fig. S1 and Table S1). To confirm the accuracy of microarray data, we examined the changes in the expression of these miRNAs following IFN-β treatment by performing quantitative reverse transcription-PCR (qRT-PCR). The findings were similar to the pattern of expression observed in the miRNA microarray analysis (Table 1). Among these miRNAs influenced by IFN-β treatment, miR-21 was pursued because of its known connection to glioma biology. Indeed, IFN-β treatment of T98 glioma cells recovered the expression of programmed cell death 4 (PDCD4), a well-known target of miR-21 (refs. 17-19; Fig. 1B).

miR-21 Overexpression in Glioma Cells, Particularly in the GICs

Previously, miR-21 was suggested to be aberrantly expressed and to be one of the major antiapoptotic factors in malignant gliomas (16, 18, 20-22). To our knowledge, we have shown, for the first time, the overexpression of miR-21 in a surgical specimen of glioblastoma by performing *in situ* hybridization (Fig. 2A-F). The *in situ* hybridization was optimized to distinguish between the areas of high (*blue*) and low expression of miR-21. The locked nucleic acid–enhanced miR-21–specific probe clearly stained the glioblastoma tissue but did not stain the normal cortex tissue. Tumor cells expressed significant amounts of miR-21, as seen at high magnification, whereas nontumoral tissue showed no expression of miR-21 (Fig. 2C and E). In contrast, neither tumor nor nontumoral tissues in the section adjacent to that hybridized with the miR-21 probe showed positive staining with the scramble probe (Fig. 2D and F). Next, we compared the miR-21 expression levels in glioma cell lines, GICs, and the normal brain tissue. The miR-21 was overexpressed in glioma cells compared with the normal brain. Notably, the amount of miR-21 was greater in GICs than in the glioma cell lines (Fig. 2G). This finding may indicate that miR-21 plays a crucial role in the initiation and progression of glioma.

IFN-β Downregulates miR-21 Transcription

Previous evidence reported by our group and others has shown that IFN-β induced growth inhibition or apoptosis in a variety of neoplasms (12, 23-25). Recently, we reported that IFN-β induced the differentiation of GICs to cells with an oligodendrocyte-like phenotype (26). In this study, we investigated the possibility that IFN-β might downregulate oncomir miR-21 in human gliomas. We compared the expression of miR-21 in IFN-β–treated and untreated glioma cells by using qRT-PCR. IFN-β treatment reduced the expression of miR-21 by ~40% to 60% in all the glioma cells tested, including the SKMG1, T98, U87, U251 glioma lines, and 0222-GIC (Fig. 3A). On the other hand, miR-21 was not affected by temozolomide, an alkylating agent commonly used in the treatment of glioma (Supplementary Fig. S2). At 4 weeks after the intracerebral inoculation of GICs, the mice received either PBS or IFN-β i.p. We previously showed that IFN-β suppressed the growth of GIC-derived intracranial tumor (26). In this study, the systemic delivery of IFN-β reduced the level of miR-21 in the tumor (Fig. 3B). The regulation of miRNA expression has been documented at the transcriptional level and RNase-mediated posttranscriptional processing (19). Therefore, we next analyzed the time course of reduction of primary *miR-21* gene transcripts (pri-miR-21), precursor miR-21 (pre-miR-21), and mature miR-21 in response to IFN-β treatment (Fig. 3C). The pri-miR-21 transcript levels decreased 6 hours after the addition of IFN-β, and began to recover at ~48 hours. Similar to these findings, the reduction of pre-miR-21 and mature miR-21 occurred as early as 6 hours. However, the recovery of pre-miR-21 began later than that of pri-miR-21. These results indicate that the decrease in the levels of miR-21 is the result of transcriptional suppression.

STAT3 Negatively Regulates miR-21 Transcription

To examine the molecular mechanisms involved in miR-21 expression, we analyzed the structure of the *miR-21* gene by studying its promoter and primary transcripts. As previously reported (27), several conserved enhancer elements were found in the consensus sequence upstream of the transcription start site of the *pri-miR-21* on the basis of TRANSFAC matrices, including Ets/PU.1, activator protein-1, serum response factor, CAAT/enhancer-binding protein-α, p53, and STAT3.[4] This suggests that highly conserved transcriptional regulatory mechanisms may operate on the *pri-miR-21* promoter (Fig. 4A). Of all these transcription factors, we focused on STAT3 in this study because IFN-β phosphorylates the tyrosine and, in part,

[4] http://www.gene-regulation.com/pub/databases.html

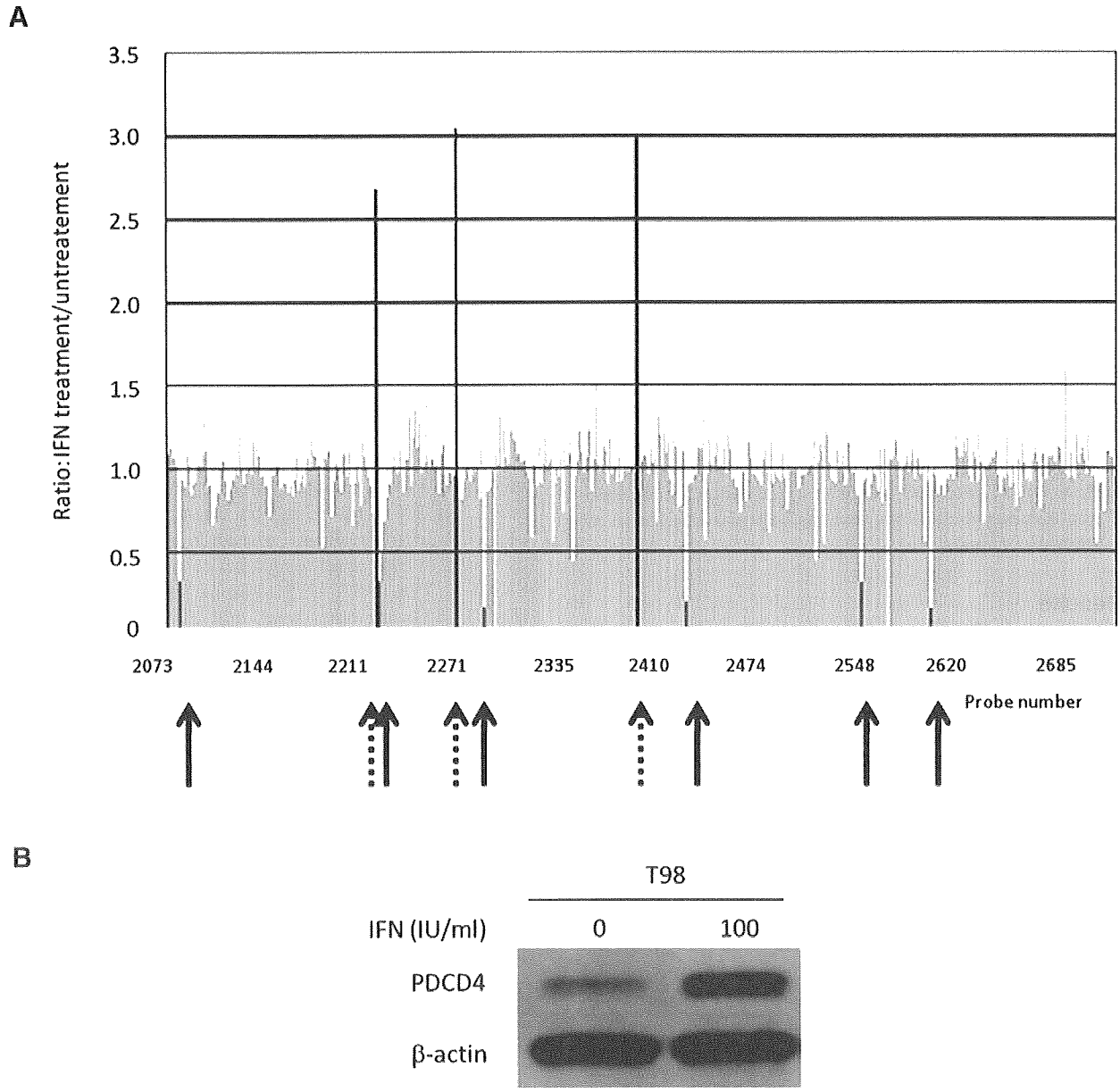

FIGURE 1. Differential miRNA expression in human glioma cells treated with IFN-β. **A.** Of 662 mammalian miRNAs spotted onto the microarray, a total of 3 overexpressing (*broken arrows*) and 6 underexpressing miRNAs (*solid arrows*) was identified in the IFN-β–treated glioma cells (see also Table 1; Supplementary Fig. S1 and Table S1). **B.** IFN-β treatment of T98 glioma cells recovered the expression of PDCD4, a well-known target of miR-21.

the serine of STAT3 in both T98 and SKMG1 glioma cells (Fig. 4B). Furthermore, a STAT3-specific inhibitory peptide increased the level of miR-21 expression and inhibited IFN-β–mediated suppression of miR-21 (Fig. 4C).

We constructed a reporter plasmid in which the full-length *pri-miR-21* promoter was fused to the 5′-end of the luciferase gene. The plasmid was transfected into T98 and SKMG1 cells. The reporter gene system displayed high basal activity in untreated cells and clearly reduced activity in response to IFN-β treatment. In contrast, the addition of the STAT3 inhibitor prior to IFN-β treatment returned the activity of the promoter to the basal level (Fig. 5A). To further determine if STAT3 is responsible for the reduction of the promoter activity, the reporter construct harboring the *pri-miR-21* promoter was cotransfected into SKMG1 cells with a STAT3-expressing plasmid, which was found to increase the total amount as well as the phosphorylation of STAT3 (Fig. 5B). As shown in Fig. 5C, the STAT3-expressing vector significantly reduced the promoter activity, and the addition of IFN-β further suppressed it.

Discussion

In this study, we hypothesized that type I IFN might regulate the expression of specific miRNAs in gliomas and that these

Table 1. Differentially Expressed miRNAs in T98 Glioma Cells Treated with IFN-β

Probe no.	MiRNA	Fold change (microarray)	Mean fold change (q-PCR*)	Chromosome location	No. of putative targets†	Connection to cancer in previous reports
Upregulated						
2269	*hsa_miR_187*	3.05	1.37 ± 0.13	18q12.2	0	↑ Thyroid tumor
2395	*mmu_miR_187*	3.00	NE	18A2	NA	NA
2218	*hsa_miR_194*	2.68	1.74 ± 0.34	1q41, 11q13.1	35	↓ Oral cancer, ↑ prostate cancer
Downregulated						
2603	*hsa_miR_100*	0.16	0.7 ± 0.15	11q24.1	6	↓ Oral cancer, ↓ ovarian cancer, ↑ hepatocallular
2285	*hsa_let_7b*	0.17	0.57 ± 0.08	22q13.31	12	↓ Lung cancer, ↓ colon cancer, ↓ breast cancer
2431	*hsa_let_7c*	0.20	0.6 ± 0.02	21q21.1	6	
2556	*hsa_let_7a*	0.32	0.66 ± 0.07	9q22.32, 22q13.31	164	
2220	*mmu_let_7a*	0.32	NE	13A5, 9A5.1	NA	NA
2083	*hsa_miR_21*	0.33	0.44 ± 0.14	17q23.1	46	↑ Glioblastoma, ↑ breast cancer

*The exprssion changes in mature miR-21, miR-187, miR-194, miR-100, and let-7a,b,c were validated in triplicate by using the LightCycler TaqMan Master and TaqMan MicroRNA assays. Values expressed as mean ± SD.
†Putative target genes were investigated by the prediction software programs, Targetscan (http://genes.mit.edu/tscan/targetscan2003.html; ref. 41), Miranda (http://www.microrna.org/microrna/getMirnaForm.do; ref. 42) and PicTar (http://www.pictar.org/) software (43). The name of common genes is listed in Supplementary Table S1.

modulations lead to antiproliferative effects. By performing initial screening by the microarray method, we observed an increase in the miR-187 and miR-194 levels and a decrease in the levels of miR-100, miR-21, and let-7 family miRNAs in response to IFN-β treatment. The biological functions and putative targets of each miRNA, except the let-7 family miRNAs and miR-21, in cancer remain unclear (Table 1). miR-187 was reported to be overexpressed in thyroid tumors (28). The level of miR-194 was decreased in colon cancer and oral cancer, but increased in prostate cancer. Therefore, it is unclear whether miR-194 acts as an oncomir or a tumor suppressor. Similarly, miR-100 was reported to be highly expressed in ovarian carcinoma and hepatocellular carcinoma, but its expression was lower in oral cancer. Let-7 is one of the first identified miRNAs. The biological functions of let-7 in animals include the regulation of stem cell differentiation, organ development, and cell proliferation and differentiation. Moreover, many let-7 family members function as tumor suppressors in a variety of cancers (29). However, there is no report suggesting that let-7 functions as a tumor suppressor in gliomas. Of the miRNAs regulated by IFN-β, we focused on miR-21 because it is one of the most well known miRNAs associated with tumorigenesis and progression in gliomas. miR-21 also modulates tumorigenesis through the regulation of genes, such as *bcl-2, PTEN, tropomyosin-1*, and *PDCD4* (17, 30-32). Indeed, IFN-β treatment of T98 glioma cells recovered the expression of PDCD4 (Fig. 1B). These results suggest that miR-21 is one of the major antiapoptotic factors. Our results showed miR-21 overexpression in a glioblastoma surgical specimen by performing *in situ* hybridization with the miR-21–specific probe, and in glioma cell lines and GICs by performing qRT-PCR. To our knowledge, this is the first report to show the expression of miR-21 *in situ* in a human glioma surgical specimen.

We found that IFN-β downregulated miR-21 in cultured glioma cells and intracranial glioma xenograft in mice. In the time course experiments, miR-21 expression was reduced as early as 6 hours after IFN-β treatment. The IFN-β treatment showed a relatively fast response in reducing miR-21 levels, suggesting that the negative regulation of miR-21 might be mediated directly by IFN-β, for example, through phosphorylation of Janus kinase/STAT. Our finding that IFN-β also suppressed the expression of pri-miR-21 and pre-miR-21 suggests that it regulates miR-21 transcription. The putative regulatory region of the *miR-21* gene is located within an intron of the overlapping transmembrane protein 49 (*TMEM49*) gene, and contains two consensus STAT3-binding sites at ~800 bp upstream from the transcription start site (33). The results of a recent study (26), similar to our findings, showed that IFN-β induces the phosphorylation of STAT3 in glioma cells and thereby activates STAT3-mediated miR-21 transcription in a luciferase reporter gene system. Our findings support the hypothesis that STAT3 activation exerts a cytostatic or antiproliferative effect in some types of cells (34-37); however, the role of STAT3 activation is debatable because its overactivation has been reported to be oncogenic in some cell lines (38, 39). Loffler et al. showed that IL-6–dependent STAT3 activates the transcription of miR-21 in multiple myeloma cells. Whereas IL-6 induces proliferation of myeloma cells, IFN-β reduces the growth of glioma cells or induces apoptosis in these cells (33). The possible explanation of this seemingly paradoxical role of STAT3 activation is that the STAT pathway is context-dependent and that various intracellular and/or environmental cues play a pivotal role in determining the outcome of pathway activation. This discrepancy may arise from the difference in cytokine stimulus and cell type (33).

An unresolved question that needs to be addressed is why the recovery of mature miR-21 occurred earlier than that of pri-miR-21 and pre-miR-21, as shown in Fig. 3C. miR-21 may form a family and possess isoforms similar to those of let-7 family miRNAs, in which the mature let-7a sequence is produced by three separate precursors (pre-let-7a-1, pre-let-7a-2, and pre-let-7a-3). Similarly, mature miR-21 could be produced by precursor(s) as well as the known pre-miR-21. One other possibility is that the maturation of miR-21 may be involved in the recovery of mature miR-21 after IFN-β treatment.

In conclusion, the downregulation of miR-21 in response to IFN-β treatment contributes to the antitumor effects of this cytokine. This is the first report demonstrating that an oncomir miR-21 is downregulated in cancer by endogenous stimulation

with a cytokine or a growth factor. This finding adds a new dimension to the anticancer mechanism of IFNs. In addition, although there is little evidence supporting a direct or immediate transcriptional regulation of miRNAs by IFNs, this study shows for the first time that miR-21 expression is negatively regulated by STAT3 activation. Our results highlight the importance of understanding the transcriptional regulation of miRNAs, which would be involved in oncogenesis.

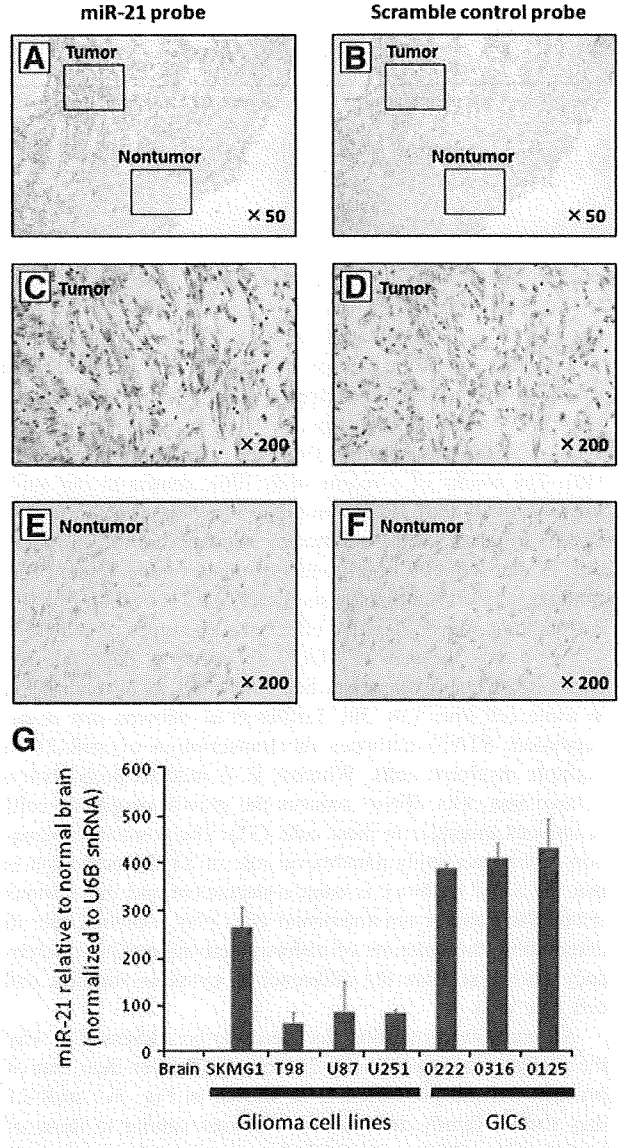

FIGURE 2. miR-21 overexpression in glioma. **A** to **F.** miR-21–specific probe and scramble control probe were hybridized *in situ* with glioblastoma tissue obtained from a surgical specimen. The miR-21–specific probe clearly stained the glioblastoma tissue but did not stain the normal cortex tissue (**A**). Tumor cells expressed significant amounts of miR-21, as observed under high magnification (**C**), whereas nontumorous tissue did not express miR-21 (**E**). In contrast, in the section adjacent to that hybridized with the miR-21 probe, neither tumor nor nontumorous tissues showed positive staining with the scramble probe (**B, D**, and **F**). **G.** qRT-PCR showed that miR-21 was overexpressed to a great extent in glioma cells than in normal brain cells. Notably, the amount of miR-21 was greater in GICs than in the glioma cell lines. Columns, mean; bars, SD (normal brain expressed as 1).

Materials and Methods

Glioma Cell Lines and Primary Tumor Sphere Cultures

We used human glioma cell lines (T98, SKMG1, U251MG, and U87MG) in this study. The source of the cell lines and the culture conditions have been reported previously (23). Glioma tissue samples were obtained from patients (nos. 0222, 0316, and 0125) undergoing surgical treatment at the Nagoya University Hospital, Nagoya, Japan, after they provided written informed consent. The procedures for the derivation of GICs were described in our recent article (26). Briefly, dissociated tumor cells were cultured in NBE media comprising neurobasal medium, with N2 and B27 supplements (Invitrogen), and human recombinant basic fibroblast growth factor and epidermal growth factor (20 ng/mL each; R&D Systems). We have previously shown that as few as 10^3 GICs could form a tumor in the brain of nonobese diabetic/severe combined immunodeficient mice (26).

Treatment

Human IFN-β (kindly provided by Toray, Kamakura, Japan) was added to the culture medium at 12 h after 2×10^5 cells were placed in a 25 cm^2 cell culture flask (BD Falcon). To examine the effect of STAT3 inhibition on miR-21 expression, we treated the cells with 50 μmol/L of the STAT3 inhibitor (PpYLKTK-mts; Calbiochem) 30 min before the addition of IFN-β. We confirmed that the STAT3 inhibitor specifically inhibited the IFN-β–mediated phosphorylation at tyrosine-705 of STAT3 (data not shown).

miRNA Microarray Analysis

We used mirVana miRNA Bioarray V2 (Ambion) containing 662 miRNAs in four copies. We treated T98 cells with IFN-β at a concentration of 100 IU/mL or with PBS for 12 h. To isolate miRNA fractions from total RNA, we fractionated and cleaned up 30 μg of total RNA by using the flashPAGE fractionator system and reagents (Ambion). Chemically synthesized oligoribonucleotides (Ambion) or purified miRNAs were labeled by using the mirVana miRNA Labeling Kit (Ambion) and amine-reactive dyes as recommended by the manufacturer. Poly(A) polymerase and a mixture of unmodified and amine-modified nucleotides were first used to append a poly-nucleotide tail. The amine-modified miRNAs were then cleaned up and coupled to *N*-hydroxysuccinimide ester–modified Cy3 or Cy5 dye (GE Healthcare). We removed the unincorporated dyes by using a second glass fiber filter–based cleaning procedure. A 3× miRNA hybridization buffer (Ambion) was added to the fluorescently labeled miRNAs, and the solution was heated at 95°C for 3 min. Slides were hybridized from 12 to 16 h at 42°C in sealed cassettes by using a water bath. Following hybridization, the slides were washed and dried before performing a high-resolution scan on a GenePix 4000B (Axon Instruments). Raw data were normalized and analyzed using Array-Pro Analyzer Version 4.5 (Media Cybernetics) to determine the signal intensity of each spot and its local background on the microarrays. We calculated the net intensity by subtracting the mean intensity of all pixels within the local background area from the mean intensity of all pixels within the spot areas. We normalized differences in net intensity between the two fluorescent dye channels in a microarray by using the local regression (loess) normalization. We selected

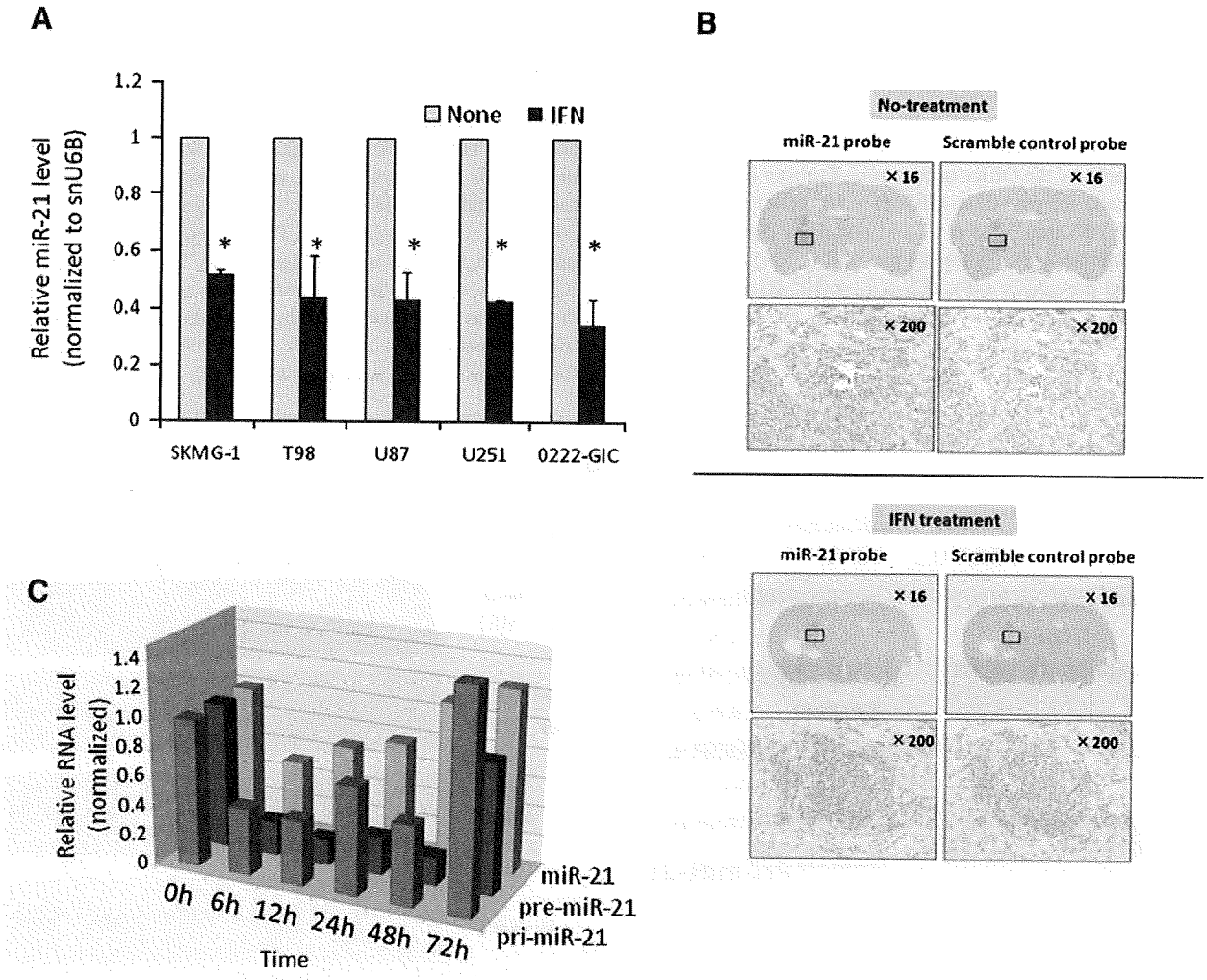

FIGURE 3. IFN-β downregulates miR-21 transcription. **A.** The expression of miR-21 in IFN-β–treated and untreated glioma cells was compared by using qRT-PCR. In all the glioma cells analyzed, IFN-β treatment reduced the expression of miR-21 by ~40% to 60%, including the cells of the SKMG1, T98, U87, and U251 glioma lines, and 0222-GIC cells. **B.** At 4 wk after intracerebral inoculation of GICs, the mice received i.p. injection of either PBS or IFN-β. IFN-β suppressed the growth of the GIC-derived intracranial tumor. In particular, the systemic delivery of IFN-β reduced the level of miR-21 in the tumor. **C.** We analyzed the time course of reduction of the levels of *pri-miR-21* gene, pre-miR-21, and mature miR-21 transcripts in response to IFN-β treatment. The levels of pri-miR-21 transcript were 0.46 ± 0.02, 0.44 ± 0.05, 0.74 ± 0.33, 0.55 ± 0.17, and 1.37 ± 0.82; pre-miR-21 levels were 0.23 ± 0.03, 0.17 ± 0.01, 0.26 ± 0.04, 0.19 ± 0.02, and 0.89 ± 0.32; and miR-21 levels were 0.53 ± 0.04, 0.69 ± 0.03, 0.78 ± 0.05, 1.11 ± 0.09, and 1.26 ± 0.16 at 6, 12, 24, 48, and 72 h, respectively. Columns, mean; bars, SD (*, $P < 0.05$).

the analyzed data by using the MicroArray Data Analysis Tool (Filgen).

qRT-PCR

Total RNA, including miRNA, was isolated by using the mirVana RNA Isolation Kit (Ambion). The analyses of mature miR-21, miR-187, miR-194, miR-100, and let-7a, let-7b, and let-7c were carried out in triplicate by using the LightCycler TaqMan Master (Roche) and TaqMan MicroRNA assays (Applied Biosystems) on a LightCycler ST300 (Roche). PCR conditions were as follows: 95°C for 10 min and 45 cycles of 95°C for 10 s, 60°C for 30 s, and 40°C for 30 s. The relative level of miRNA expression was calculated by the 2-ΔΔCt method. The data were normalized to the expression of U6B small nuclear RNA. In some assays, samples from the normal brain tissue were used as a calibrator, whereas in others, untreated samples were used.

To quantify the pri-miR-21 and pre-miR-21 expression, we treated the isolated RNA with DNase and reverse-transcribed it using the Transcriptor First Strand cDNA Synthesis Kit (Roche). The LightCycler-FastStart DNA Master SYBR Green I kit (Roche) was used for real-time PCR applications. The primer sets for pri-miR-21 and pre-miR-21 qRT-PCR were 5′-TTTTGTTTTGCTTGGGAGGA-3′ and 5′-AGCAGACAGTCAGGCAGGAT-3′, and 5′-TGTCGGGTAGCTTATCAGAC-3′ and 5′-TGTCAGACAGCCCATCGACT-3′, respectively. The PCR conditions were as follows: 95°C for 15 min, and 40 cycles of 95°C for 10 s, 60°C for 10 s, and 72°C for 10 s.

Western Blotting

Cell lysis and immunoblotting were done as described previously (23). Antibodies against the following proteins were used: PDCD4 (ab51495; Abcam), phosphorylated STAT3 (p-Ser727

and p-Tyr705), STAT3 (Cell Signaling), and β-actin (AC-15; Sigma-Aldrich).

Intracranial Glioma Xenograft and IFN-β Treatment

Animal experiments were done according to the principles described in the Guide for the Care and Use of Laboratory Animals prepared by the Office of the Prime Minister of Japan. We stereotactically injected 0316-GICs (1×10^5 cells) resuspended in 5 μL of PBS into 5- to 6-wk-old nonobese diabetic/severe combined immunodeficient female mice (SLC, Shizuoka, Japan) as described previously (40). IFN-β (2×10^5 IU/animal) was given i.p. at 4 wk after tumor inoculation. The control mice received PBS. Treatments were repeated at 24-h intervals for a total of five doses.

In situ *Hybridization*

Tissues were fixed with Tissue Fixative (Genostaff), embedded in paraffin, and sectioned at 6 μm. For performing *in situ* hybridization, the tissue sections were deparaffinized with xylene, and rehydrated using a series of ethanol washes and PBS. The sections were fixed with 4% paraformaldehyde in PBS for 15 min and then washed with PBS. They were then treated with 10 μg/mL of Proteinase K in PBS for 30 min at 37°C, washed with PBS, refixed with 4% paraformaldehyde in PBS, washed again with PBS, and placed in 0.2 mol/L of HCl for 10 min. After washing with PBS, the sections were acetylated by incubation in 0.1 mol/L of triethanolamine-HCl (pH 8.0) and 0.25% acetic anhydride for 10 min. After washing with PBS, the sections were

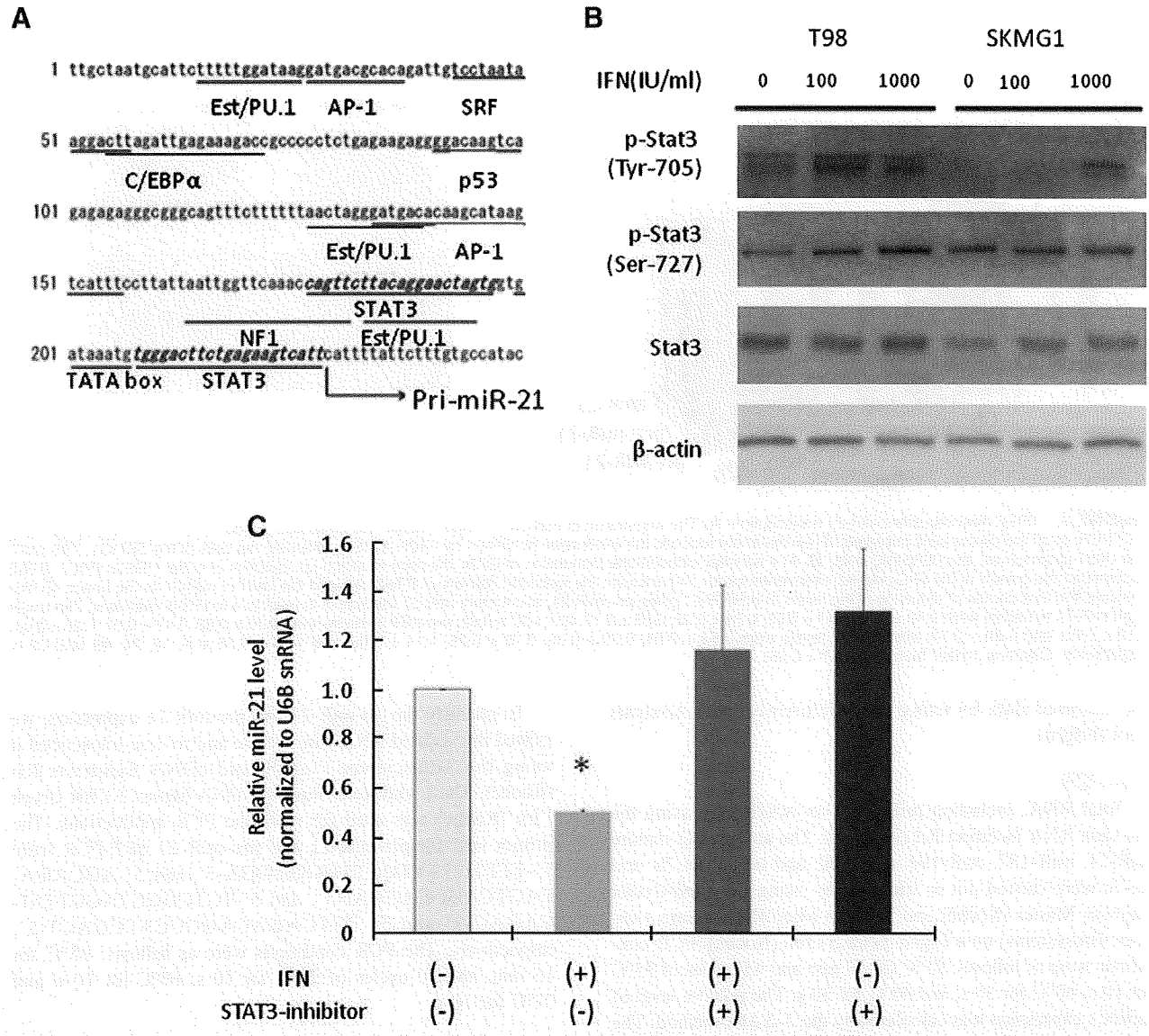

FIGURE 4. STAT3 negatively regulates miR-21 transcription. **A.** Consensus sequence upstream of the transcription start site of the *pri-miR-21* obtained using TRANSFAC matrices (http://www.gene-regulation.com/pub/databases.html). **B.** IFN-β phosphorylates tyrosine and, in part, serine residues of STAT3 in both T98 and SKMG1 glioma cells. **C.** Treatment with a STAT3-specific inhibitory peptide increased the level of miR-21 expression and inhibited IFN-β–mediated suppression of miR-21 (*, $P < 0.05$).

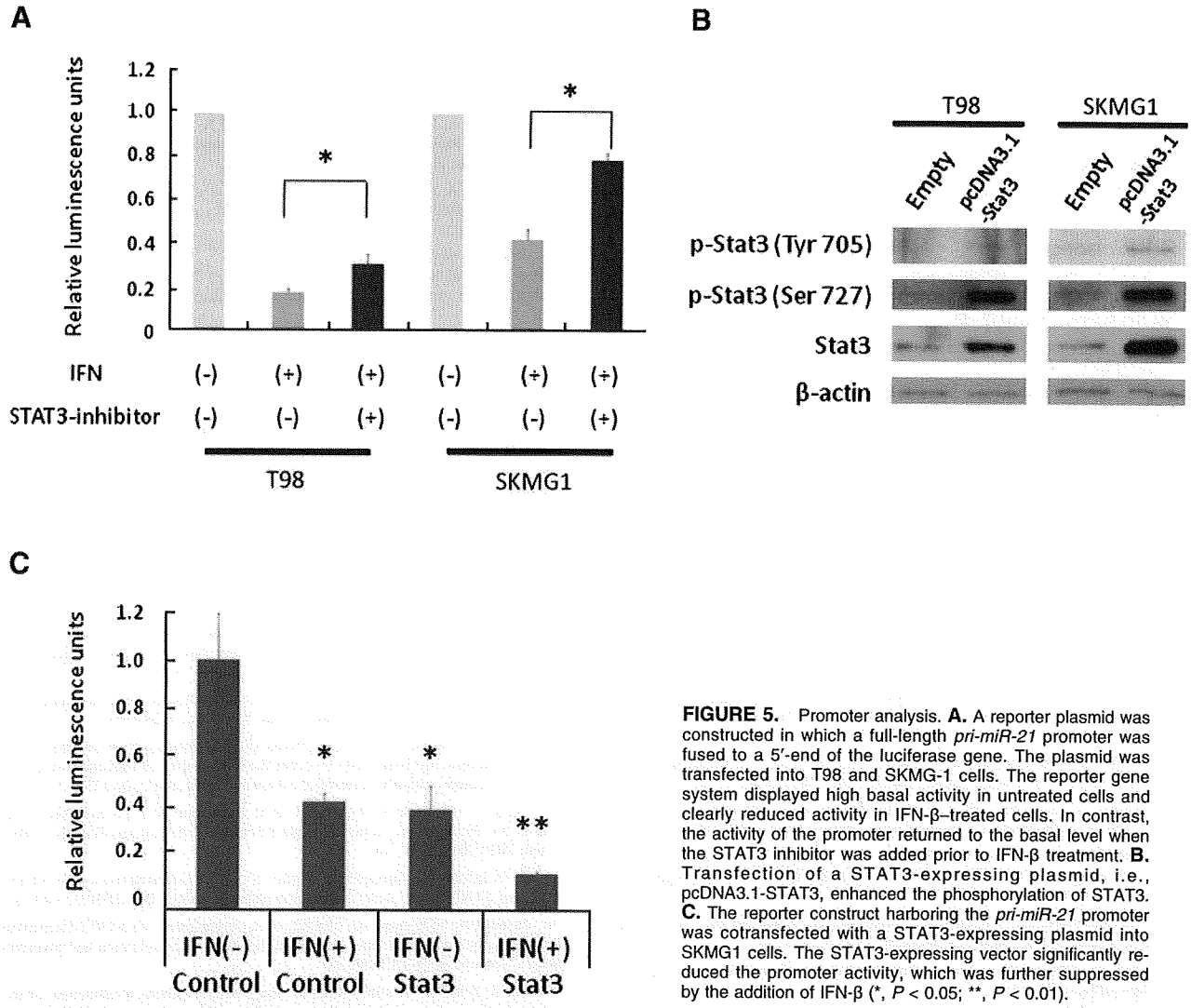

FIGURE 5. Promoter analysis. **A.** A reporter plasmid was constructed in which a full-length *pri-miR-21* promoter was fused to a 5′-end of the luciferase gene. The plasmid was transfected into T98 and SKMG-1 cells. The reporter gene system displayed high basal activity in untreated cells and clearly reduced activity in IFN-β–treated cells. In contrast, the activity of the promoter returned to the basal level when the STAT3 inhibitor was added prior to IFN-β treatment. **B.** Transfection of a STAT3-expressing plasmid, i.e., pcDNA3.1-STAT3, enhanced the phosphorylation of STAT3. **C.** The reporter construct harboring the *pri-miR-21* promoter was cotransfected with a STAT3-expressing plasmid into SKMG1 cells. The STAT3-expressing vector significantly reduced the promoter activity, which was further suppressed by the addition of IFN-β (*, $P < 0.05$; **, $P < 0.01$).

dehydrated using a series of ethanol washes. Hybridization was done with either the locked nucleic acid–enhanced miR-21 probe (5′-TCAACATCAGTCTGAATAAGCTA-3′; Exiqon) or a scramble probe (5′-GTGTAACACGTCTATACGCCCA-3′) at concentrations of 18 nmol/L in the Probe Diluent (Genostaff) at 50°C for 16 h. After hybridization, the sections were washed in 5× HybriWash (Genostaff; equivalent to 5× SSC) at 50°C for 20 min and then in 50% formamide, 2× HybriWash at 50°C for 20 min. Subsequently, the sections were washed thrice with 2× HybriWash at 50°C for 20 min, and once with TBS Tween 20 (TBST; 0.1% Tween 20 in TBS). After treatment with 0.5% blocking reagent (Roche) in TBST for 30 min, the sections were incubated with anti–DIG-AP conjugate (Roche) diluted 1:1,000 with TBST for 2 h. The sections were washed twice with TBST and then incubated in 100 mmol/L of NaCl, 50 mmol/L of $MgCl_2$, 0.1% Tween 20, and 100 mmol/L of Tris-HCl (pH 9.5). Coloring reactions were done using nitroblue tetrazolium-5-bromo-4-choloro-3-indolylphosphate, an alkaline phosphate color substrate. The sections were counterstained with Kernechtrot stain solution (Muto, Tokyo, Japan), dehydrated, and then mounted with Malinol (Muto).

Luciferase Reporter Assay

The miR-21 promoter/enhancer region was amplified by PCR from human genomic DNA using the primers 5′-TTTGGTACCTTGCTAATGCATTCT-3′ and 5′-TTTAGATCTAGTTCA GCTATGGTAAGAGC-3′ and inserted into the *Kpn*I and *Bgl*II sites of pGL3-Enhancer vector (Promega) immediately downstream of the luciferase gene to form a pGL-miR-21 promoter/enhancer construct. The overexpression of STAT3 in the cells was achieved by transfection with pcDNA3.1-STAT3 that was provided by Dr. Takeshi Senga (Department of Tumor Biology, Nagoya University School of Medicine, Nagoya, Japan). The SKMG1 and T98 cell lines were seeded in 24-well plates for 24 h and then transfected with 1 μg of pGL-miR-21 promoter/enhancer construct with or without pcDNA 3.1-STAT3 for 48 h.